First calibrations and studies of the BabyMIND detector

B. Martinez
DPNC, Geneva University

September 2016

Contents

1 Introduction

Neutrino are the subject of many questions in particle physics of the early XXI^e century. Indeed they are the only sector which the Standard Model is unable to fully describe.
One way to prove that there is something beyond the Standard Model is to study neutrino oscillation. That's the main goal of the T2K experiment which try to give a better understanding of the physics of these seemingly exotic particles. The idea of T2K is to analyze a neutrino beam near its source and far of it. Then, by comparing the characteristics of the beam at these two point, one can observe neutrino oscillations. However, it requires to have a good knowledge of the neutrino cross-sections. A new detector, WAGASCI, was designed espacially to study the cross-section of the neutrino in water and hydrocarbon[1]. Eventually, another project was born to complete WAGASCI, the Baby MIND. The Baby MIND was designed to as a sub-detector of WAGASCI to reduce wrong-sign background. However, it is an independant detector than can be use in other experiments. By design, the Baby MIND is conceived to achieve high charge identification efficiencies in the energy range relevant to the T2K beamline (i.e. with a neutrino peak around 700 MeV). T2K analyses cover both ν_μ disappearance and ν_e appearance for which a good understanding of the neutrino beam and it's interactions with detectors near and far is required. Baby MIND will contribute to a better understanding of the neutrino cross-section by doing high charge identification efficiencies.
In this report, we will describe the T2K experiment and the place and purpose of the Baby MIND in it. Then, we will cover the detector itself : its design, conception, simulation and tests. We will describe in more details the electronic of the detector and finish by by beam tests carried out during the summer 2016 to characterise it.

2 Theory

Neutrinos are in many ways special particles. First, they are several orders of magnitude lighter than all other fermions. Secondly they are totally neutral : no electric charge and no color charge. They interact only through weak interactions and with a ridiculous small cross section[2]. They are very difficult to detect since they can travel through the Earth without interacting.
A better understanding of neutrino physics could solve some of the biggest question of the Physics of the early XXI^e century such as the asymmetry of the matter/antimatter repartition in the universe or even the dark matter.

[1] water and hydrocarbon are the target of the neutrino beam

[2] Neutrinos produced in nuclear reactors with an energy E_ν $1MeV$ have a cross-section of σ $10^{-44}cm^2$.

2.1 Neutrino Beam

A way to pass through this problematic of poor interaction statistic is to produce a neutrino beam. The huge quantity of neutrino in the beam allows to overcome the weak probability of interaction. Here, we will explain how a neutrino beam such as the one provided at J-PARC is produced and how it is then detected.

Pion Decay

The idea is to collide a proton beam on a target. A proton is basically an atom of Hydrogen without its electron (so H^+), it is then relatively easy to produce a beam of protons. When this beam hits a target, the protons will produce some pions which will decays through :

$$\pi^+ \rightarrow \mu^+ + \nu_\mu \tag{1}$$

The neutrino are produced in the same direction of the incoming pion. Using a magnetic horn, one can focus the pion beam in the good direction. Then, the beam will pass through a decay tunnel within which the pions will decay into the neutrinos. At the end, we can have a well defined neutrino beam.

Lepton Production

The detection of the neutrino is done mostly by the observation of the Charge Current :

$$\nu_l + n \rightarrow l + p \tag{2}$$

This is not the neutrino that is directly detected, but the charged lepton it produced through its interaction with matter. This is by measuring the properties of the leptons that one can estimate the ones of the original neutrino.

Cherenkov Effect

This effect is the main detection method for the far detector of T2K (Super-Kamiokande). In fact, when a charged particle travels through a dielectric medium at a speed greater than the phase velocity of the light in that medium, it emits an elecromagnetic radiation. This effect is known as the Cherenkov effect. As the emitted light cannot be faster than the charged particle, the light emitted has the form of a cone. It is analog to the sonic boom a supersonic plane produce.
This light can the be detected to measure the properties of the charged particle.

2.2 Neutrino Masses and Oscillations

The Standard Model as we know it is shown in the left Figure 1. As we can see, there are 3 flavour of neutrino, each corresponding to a lepton flavour. However, the neutrino part is incomplete, as shown on the right part. In fact the

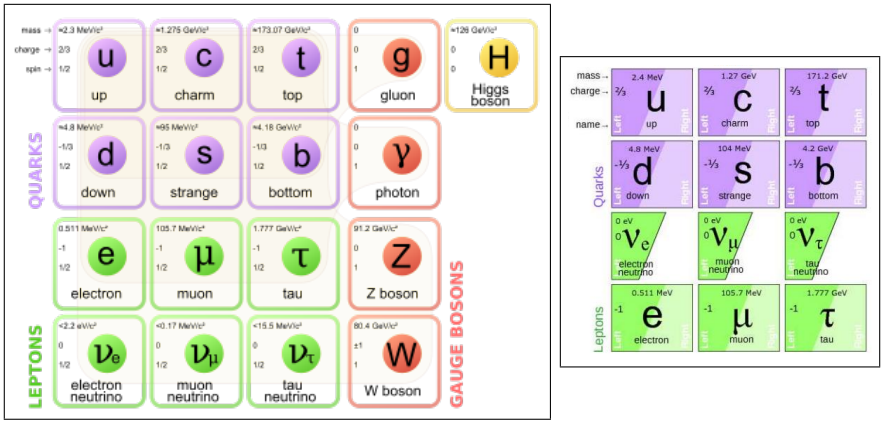

Figure 1: Left : the standard model. Right : A closer look to the leptons and the missing right chirality of the neutrinos.

right-handed neutrinos have never been observed.
The fact is that the standard model predicts that the neutrinos have zero masses. However, we know that they have masses, which means the standard model is incomplete. A manner to prove this is through the neutrino oscillation.
The idea behind the neutrino oscillation is that the neutrino flavor state we know (ν_e,ν_μ,ν_τ) are not mass eigenstates but a superposition of such states :

$$\begin{pmatrix} \nu_e \\ \nu_\mu \\ \nu_\tau \end{pmatrix} = \begin{pmatrix} U_{e1} & U_{e2} & U_{e3} \\ U_{\mu 1} & U_{\mu 2} & U_{\mu 3} \\ U_{\tau 1} & U_{\tau 2} & U_{\tau 3} \end{pmatrix} \begin{pmatrix} \nu_1 \\ \nu_2 \\ \nu_3 \end{pmatrix} \tag{3}$$

Where U is a 3 x 3 unitary matrix called the PMNS matrix[3] which mixes the neutrino states. It can be more simple to decompose it in the 3 rotation matrices :

$$U = \begin{pmatrix} 1 & 0 & 0 \\ 0 & c_{23} & s_{23} \\ 0 & -s_{23} & c_{23} \end{pmatrix} \begin{pmatrix} c_{13} & 0 & s_{13}e^{-\delta_{CP}} \\ 0 & 1 & U_0 \\ s_{13}e^{-\delta_{CP}} & 0 & c_{13} \end{pmatrix} \begin{pmatrix} c_{12} & s_{12} & 0 \\ -s_{12} & c_{12} & 0 \\ 0 & 0 & 1 \end{pmatrix} \tag{4}$$

With $c_{ij} = cos(\theta_{ij})$,$s_{ij} = sin(\theta_{ij})$, δ_{CP} the Dirac type CP phase which is irreducible[4]
The theory postulated by Pontecorvo is that the Neutrino flavor can change through time and distance. It means you can have a ν_e at space-time location A and a ν_μ at a space-time location B. This phenomenon is called oscillation. The explication is that the mass eigenstates propagates each with a different

[3] from the name of its inventors Pontecorvo-Maki-Nakagawa-Sakata

[4] this is a property of Group Theory who says that there are $\frac{(n-1)(n-2)}{2}$ irreducible phase for a n x n matrix.

phase velocity, leading to different combinaisons (the flavour states) along their trip.
We know that neutrino can be produced in weak interaction. Here, this is the flavor states that interacts. After a time t it becomes :

$$|\nu_\alpha >_t = \sum_{i=1}^{3} U^*_{\alpha i} e^{-E_i t} |\nu_i > \tag{5}$$

With ν_α the flavor eigenstate and ν_i the mass eigenstate. It means the probability that a neutrino α oscillates in β after t is :

$$| < \nu_\beta | \nu_\alpha > |^2 = | \sum_{i=1}^{3} U^*_{\alpha i} e^{-E_i t} \sum_{j=1}^{3} U_{\beta j} e^{E_j t} |^2 = | \sum_{i=1}^{3} \sum_{j=1}^{3} U^*_{\alpha i} U_{\beta j} e^{-i(E_i - E_j)t} |^2 \tag{6}$$

Using $E_i = \sqrt{p^2 + m_i^2} = p + \frac{m_i^2}{2p}$ and $E_i - E_j = \frac{m_i^2 - m_j^2}{2p} \cong \frac{\delta m_{ij}^2}{2E}$ and $t = \frac{L}{\beta}$ with $\beta \cong 1$, we can rewrite :

$$| < \nu_\beta | \nu_\alpha > |^2 = | \sum_{i=1}^{3} \sum_{j=1}^{3} U^*_{\alpha i} U_{\beta j} e^{-i \frac{\delta m_{ij}^2}{2E} L} |^2 \tag{7}$$

So, measuring neutrino oscillation gives a direct measure of the U matrix characteristics and neutrino masses. Observing such oscillation would then prove that the standard model is not complete and could provide more information about neutrino physics. That's why experiments like T2K have been built.

3 Tokai to Kamiokande experiment

The Baby MIND is a sub-detector of the WAGASCI experiment which will be detecting neutrinos from the T2K beamline. The main goal of this section is to explain in which context BabyMIND exists, so we won't go into great details but rather explain the main principles of this experiment.
T2K [4, 5, 6] is a long-baseline neutrino experiment which studies neutrino oscillations. The idea is to produce a beam and to measure his composition in neutrino near the production (Tokai) and at 295 km from the source (Kamiokande). Then, by measuring rates at near and far sites and comparing with predictions, one can analyze appearance and disappearence of neutrino flavour. The study of these neutrino appearance/disappearance leads to the observation of neutrino oscillation.

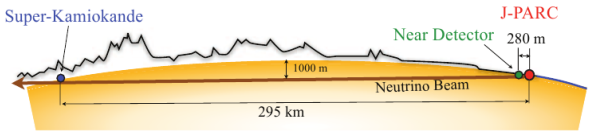

Figure 2: T2K Beam line [2]

3.1 Neutrino Beam from J-PARC

J-PARC was constructed at Tokai, Ibaraki (Japan) and consists of three accelerators :

1. a linear accelerator (LINAC)
2. a rapidcycling synchrotron (RCS)
3. the main ring (MR)

At first, the LINAC accelerates an H^- beam up to 400 MeV[5]. The beam is converted into a proton beam at the RCS injection. This is achieved using charge-stripping foils which separate negatives charges from the ions, leaving only the protons.
Then, the proton beam is accelerated up to 3 GeV by the RCS. Only about 5% of the bunches produced by the RCS are sent to the MR. The remaining bunches are supplied to the muon and neutron beamline in the Materials and Life Science Experimental Facility (MLF)[6].
The protons injected in the MR are accelerated up to 30 GeV. The beam can be fast extracted or slow extracted. In our case, we are interested in the fast extraction[7]. For each acceleration cycle, the beam is extracted as a spill which contains 8 bunches of about 5μs.
After being extracted from the MR, the beam travels to an arc section to align it toward Kamioka, it will hit a target to produce a pion beam. The pions will then mainly decay in muons and neutrinos.

After the extraction, the beam has the caracteristics described in Table 1.

Table 1: Design characteristics of the beam. The recorded beam power is currently around 400 kW.

Beam power	750 kW
Beam kinetic energy	30 GeV
Beam intensity	3 x 10^{14} proton/spill
Number of bunches	8/spill
Spill width	5 μs
Spill cycle	0.5 Hz

After the arc, the beam will reach the target station (TS). The target is a graphite rod 91.4 cm long and 2.6 cm diameter. When the protons collide with the target, they produce secondary particles, mostly pions (which are what we

[5] 181 MeV for now
[6] MLF is another Facility of J-PARC studying very intense pulsed muon and neutron beams
[7] slow extraction is for an hadron beamline

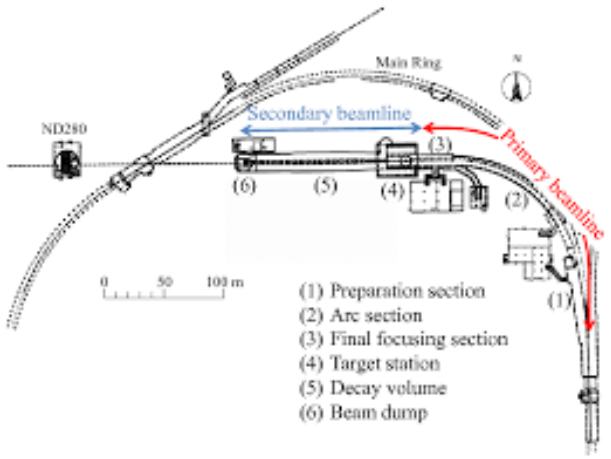

Figure 3: Scheme of neutrino production from proton beam [4]

need for the neutrino beam) but also kaons (which will contaminate our final neutrino beam).
Three successive magnetics horns[8] are used in the beamline. The first collects the pions (and other secondary particles) generated by the target, which is installer in its inner conductor. The two following horns focus the pions. They run with an operating current of 320 kA and display a maximum field of 2.1 T. This increases the neutrino flux in the far detector by a factor of 16 (compared with horns at 0 kA), considering a peak energy of 0.6 GeV. The polarity of the horns' current can be adapted to focus positive or negative charge which allow us to choose a beam of neutrino or anti-neutrino.
The produced pions will decay in flight inside the decay volume (96 m long, 1500 m^3) which is filled with helium (1 atm) to reduce pion absorption and to suppress tritium and NOx production by the beam. The neutrino are produced by pion decay[9].
At the end of the decay volume sits the beam dump. Its purpose is to stop the remaining hadrons and low energy muons. It is composed of large graphite blocks which allows only muons with energy higher than 5.0 Gev to pass through, along with the neutrinos of course.
The muons are detected by a muon monitor. As neutrino are mainly produced along with muons, the neutrino beam profile can be determined by the muon beam profile.
Here we aim to have a ν_μ or $\overline{\nu_\mu}$ beam as pure as possible. However, because of the decay of kaons and muons before the beam dump, there will be a small ν_e or $\overline{\nu_e}$ contamination. This contamination is less than 1% o the flux. However there is another kind of contamination. In fact the magnetical horns can't focus

[8] Each magnetic horn consists of two coaxial (inner and outer) conductors which encompass a closed volume
[9] see section 2.1

100% of the beam so there will be a wrong sign contamination which will result in a $\overline{\nu}$ contamination in ν beam and vice-versa.

Neutrino	Decay	Fraction (%)
ν_μ	$\pi^+ \to \mu^+\nu_\mu$	73
	$K^+ \to \mu^+\nu_\mu$	13
	$K^+ \to \pi^0\mu^+\nu_\mu$	12
	$K^0 \to \pi^0\mu^+\nu_\mu$	2
	$\mu^- \to e^-\overline{\nu_e}\nu_\mu$	0.02
$\overline{\nu_\mu}$	$K^- \to \mu^-\overline{\nu_\mu}$	42
	$K^- \to \pi^0\mu^-\overline{\nu_\mu}$	21
	$\pi^- \to \mu^-\overline{\nu_\mu}$	14
	$K^0 \to \pi^0\mu^+\overline{\nu_\mu}$	13
	$\mu^+ \to e^+\nu_e\overline{\nu_\mu}$	9
ν_e	$K^+ \to \pi^0e^+\nu_e$	50
	$\pi^+ \to e^+\nu_e$	38
	$K^0 \to \pi^-e^+\nu_e$	8
	$\mu^+ \to e^+\nu_e\overline{\nu_\mu}$	4
$\overline{\nu_e}$	$K^- \to e^-\overline{\nu_e}$	57
	$K^0 \to \pi^+e^-\overline{\nu_e}$	33
	$\pi^- \to e^-\overline{\nu_e}$	9
	$\mu^- \to e^-\overline{\nu_e}\nu_\mu$	2

Table 2: Fraction of each decay mode which contributes to neutrinos under the flux peak (0.4 GeV $\leq E_\nu \leq$1.0 GeV)

Off-Axis Beam

For the first time in a search for neutrino oscillations, the T2K experiment employs an off-axis method. In fact, the energy of a neutrino emitted in the two-body pion (and kaon) decay is :

$$E_\nu = \frac{m_\pi^2 - m_\mu^2}{2(E_\pi - p_\pi cos(\theta))} \tag{8}$$

with θ the angle between the neutrino direction and the incoming pion. In fact, the neutrino energy is only weakly dependant on the momentum of the pion. If we vary the angle θ, we will see neutrino with a narrow spread in energy.

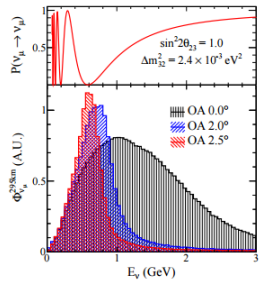

Figure 4: Muon neutrino survival probability at 295 km (far detector) and the neutrino fluxes for different off-axis angle. [6]

In the case of T2K, a 2.5^0 off-axis has been set to have a peak energy at 0.6 GeV at the far detector, that is near the expected first oscillation maximum (see Figure4). In this case we have a higher neutrino flux at the desired energy than on a on-axis situation.

3.2 Far detector

Super-Kamiokande, often called Super-K, is the actual far detector of the T2K experiment. It is located 295 km west of the beam source in the Mozumi mine of the Kamioka Mining and Smelting Company, near the village of Higashi-Mozumi, Gifu, Japan.

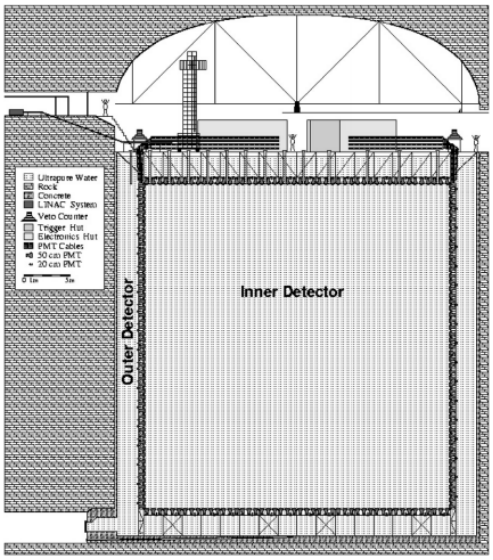

Figure 5: Cut of the Super-K experiment [7]

The detector cavity lies 1 km deep within the Mt. Ikenoyama. Super-K is a huge Cherenkov detector. It consists of a cylindrical water tank, with a capacity of 50 kton, within which about 13000 photomultiplier tubes (PMTs) image neutrino interactions.
Super-K has been running since 1996. It had produced a lot of data and in this sense, it is a well-known detector which whose behaviour is well understood.

Super-K a cylindrical detector which consists of two major volumes, an inner (ID) and an outer (OD) detector separated by a cylindrical stainless steel structure. The ID is a space of 33.8 m diameter and 36.2 m height which contains the 50 ktons of water. Its inner walls are recovered by more than 11000 inward facing PMTs of 50 cm diameter.
The OD encloses the ID. Only 2 m thick separate separate them. One can find about 1900 PMTs outward-facing PMTs of 20 cm diameter on the inner walls of the OD.
ID and OD are bounded by a cylindrical structure of stainless steel and plastic sheet which optically separate the two detector.

Neutrino interactions inside the water will produced charged particles. These particles, above a certain energy threshold, will go faster than the light in the water. They will then produce a cone of Cherenkov (see Section 2.1.3). When the photons reach the PMTs on the walls, they produce a ring-shaped hit pat-

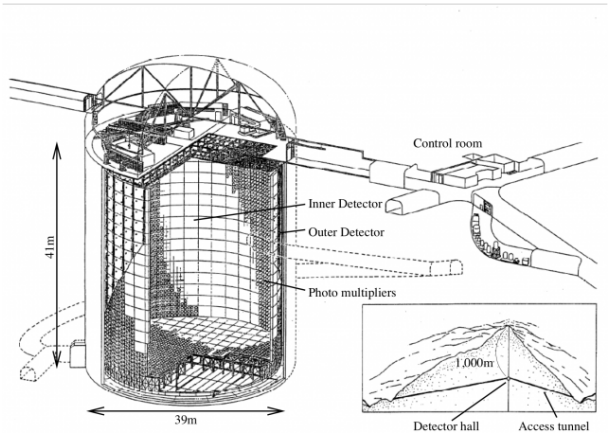

Figure 6: Scheme of the Super-K experiment [4]

tern.

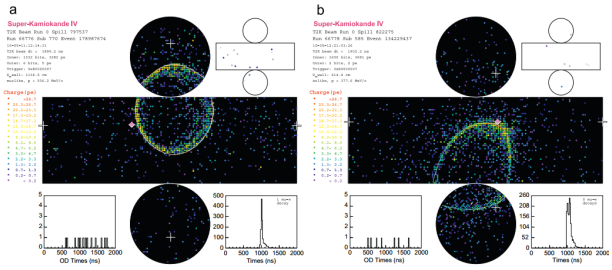

Figure 7: Example of reconstructed event for (a) a muon-like ring and (b) an electron-like ring. Each show the detector unrolled into a plane. Each colored point represents a PMT with the color corresponding to the amount of charge.The reconstructed cone is shown as a white line. One can find the reconstructed vertex because of the white crosses. The diamonds marks the spot where a ray coming from the vertex and heading in the same direction of the beam would hit the detector wall. The sedondaries figures in the upper right show the same hit map for the OD[4].

In Figure 7, we have 2 examples of event in Super-K. As the muons (a) are massive, there are not deviated a lot when they propagate inside the water so the ring they produce is sharp. On the other hand, electrons (b) are light and they undergo several scattering during their travel. For this reason, their ring is less neat than the muons'. These characteristics are useful because the point

of Super-K is to distinguish ν_μ events to ν_e events and compare the results with the ones of the near detectors to observe neutrino oscillations.
The strategy is then to count charged-current quasi-elastic interactions for ν_μ and ν_e. These interactions will produce leptons of their respective flavor as you can see on Figure 8.

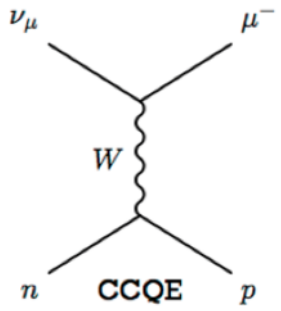

Figure 8: CCQE diagram for muons. Same for electrons

As we have already seen, it is possible to differenciate muons and electrons events. The event reconstruction software of Super-K uses this difference between sharp and fuzzy to determine which particle is involved.

3.3 Near detectors

In order to obtain valuable results for the T2K experiment, it is very important to characterize the neutrino beam at J-PARC with as low uncertainty as possible. If this characterisation is done, the comparison between the predicted (based on the results of the "source" : J-PARC) and measured observables would make more sense. That's why it is crucial to have detectors near the "source" of the beam.
These detectors are sets in the ND280[10] pit. The near detectors should give us more information on the neutrino flux and the neutrino cross-section. Aside from the energy spectrum, they should also provide information on contamination ($\overline{\nu}$ in ν beam[11] and ν_e contamination) as a function of the neutrino energy. These informations are crucial since, for example, if we detect a ν_e at Super-K, we need to know if it comes from a ν_μ that oscillated or if it was a part of the initial ν_e contamination. For now, there is two near detectors : INGRID and the ND280 complex. The near detectors should be complemented in the next years by the WAGASCI project which includes the BabyMIND detector.[12].

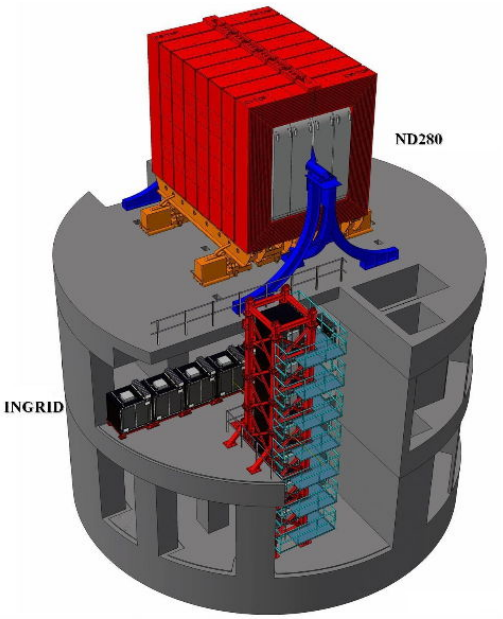

Figure 9: Localisation of the near detectors in the ND280 pit [3]. The block at the top is generally identified at ND280 and the other colored blocks as INGRID.

[10] acronyme for Near Detector and the 280 comes from the pit is at 280 m from the source
[11] wrong-sign contamination
[12] see section 3.3 for WAGASCI and 4 and 5 for BabyMIND

3.3.1 INGRID

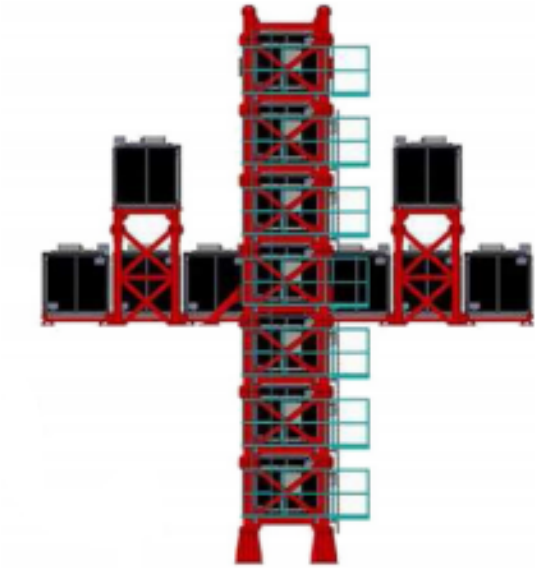

Figure 10: The INGRID detector [4]

INGRID stands for Interactive Neutrino GRID. The INGRID detector cover a large area, but its center is on-axis. That's why it is often referred as an on-axis detector. It is installed in the ND280 pit (see Figure 9). This detector monitors directly the neutrino beam direction and intensity *via* neutrino interactions in iron.
INGRID consists of 16 identicals modules arranged like a cross as in Figure 10. There is two identical groups on the vertical and horizontal axis of 7 modules each and two additional separate modules outside the main cross. The center of the cross corresponds to the beam center. The two off-axis modules are here to check the axial symmetry of the neutrino beam.
An INGRID modules is composed of 9 iron plates and 11 tracking scintillator planes arranged like in Figure 11. Those plates are surrounded by the veto planes. They are scintillator planes which have the mission to reject interactions taking place outside the module. The iron plates are 124 x 124 x 6.5 cm^3 each. The tracking planes consists of 24 x 24 scintillator bars with each scintillator bar of 1.0 x 5.0 x 120.3 cm^3. On the other hand, the veto planes are made of 22 scintillator bars segmented in the beam direction. The scintillator bars of th bottom veto planes make 1.0 x 5.0 x 111.9 cm^3 while the scintillator bars of th top, right and left veto planes make 1.0 x 5.0 x 129.9 cm^3. The bars are made of polystyrene (doped with 1% PPO and 0.03% POPOP) surrounded by a thin white reflective coat (TiO_2 infused in polystyrene) within which a 1 mm

diameter WLS fiber is inserted (see [8]). At the both end of the bar, the fiber is connected to an MPPC. You can find characterization of them in [9, 10].

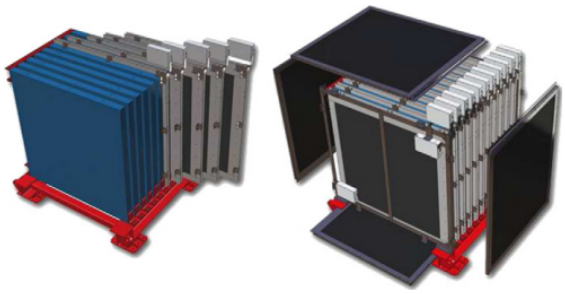

Figure 11: The INGRID modules. On the left, one can see the tracking plates (in blue) and iron plates. On the right, the veto planes are illustrated in black [4].

As a result [11], INGRID shows that the neutrino beam remains stable and is able to measure the beam center within a 10 cm precision[13]. Figure 12 shows results of the detector.

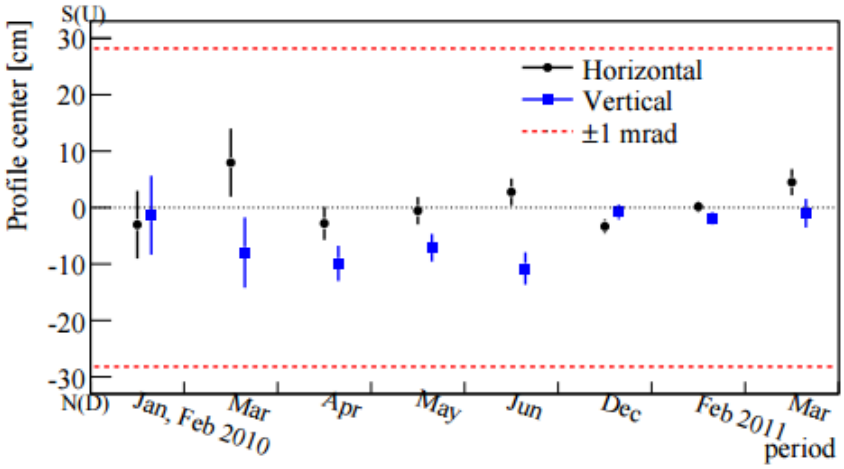

Figure 12: History of the neutrino beam center from January 2010 to March 2011 [11].

It is relevant to say that an extra module, called the Proton Module, was

[13]This corresponds to 0.4 mrad 280 m from the origin.

added to INGRID. Its purpose is to detect with good efficency the muons along with the protons produced by the neutrino beam in INGRID. Doing this, it has to identify the quasi-elastic channel for comparison with Monte-Carlo simulations.
The Proton Module is like the other modules without the iron plates[14]. The Proton Module is placed in the center of the cross, between the vertical and the horizontal axis. Typical events in INGRID and the Proton Module are shown in Figure 13.

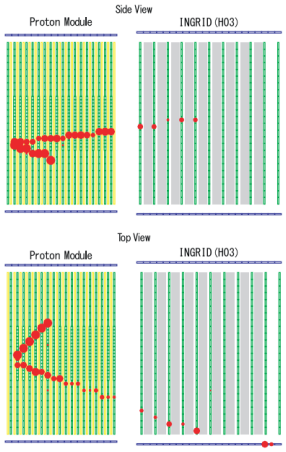

Figure 13: This is a typical neutrino event in both INGRID and the Proton Module. A neutrino enters from the left and interact within the module. This interaction produces charged particles which can be detected by the scintillator bars. Their tracks are shown as the red dots. We can see one of them escapes the Proton Module and penetrates the central INGRID horizontal module. As each green cell is a scintillator, the blue ones indicate a veto scintillator while the grey bars stand for the iron plates. The size of the red dots indicates the observed signal in the corresponding cell [4].

[14] the scintillator bars have other dimensions

3.3.2 ND280

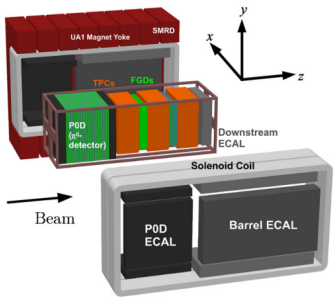

Figure 14: Exploded view of the ND280 off-axis detector[4].

ND280 is an off-axis detector located as shown in Figure 9 to monitor the beam with a 2.5^0 off-axis angle. It is a tracking detector composed of various specified modules within which one can count :

1. **UA1 magnet** The UA1 encloses the other modules, providing a 0.2 T magnetic fields inside the detector. This magnetic fiel is important to measure momenta with good resolution and to determine the sign of the charged particle produced by neutrino interactions[15].

2. **Pi-zero detector (POD)** The objective of the POD is to measure Neutral current process[16] on a water target with the same neutrino flux which will reach Super-K.

3. **Time Projection Chamber (TPC)** The TPCs assure three functions in ND280 : determine the number and orientation of charged particles passing through, measure the momenta of charged particle thanks to the magnetic field and determine the event rate as a function of the neutrino energy. Altogether, these informations allow to determine the abundance of ν_e in the beam.

4. **Fine Grained Detector (FGD)** The two FGD have two role. They first provide a target mass for neutrino interaction and then are a tracking for charged particles coming from the interaction vertex.

5. **Electromagnetic Calorimeter (ECal)** The ECal surrounds the POD, TPCs and FGDs. It is almost perfectly hermetic to the particles exiting the inner detectors. It completes the other detector by detecting photons, measuring their energy and direction, as well as charged particles, again measuring energy and direction which allow their identification. The ECal has a key function of reconstructing π^0 produced in the inner detectors.

[15] and then determine if it was an neutrino or an anti-neutrino
[16] $\nu_\mu + N \rightarrow \nu_\mu + N + \pi^0 + X$

6. **Side Muon Range Detector (SMRD)** The first function of the SMRD is to records muons escaping with high angle (w.r.t. the beam) direction and measure their momenta. Then it triggers the muons coming from cosmic rays penetrating the ND280 detector. Finally it helps at the identification of beam-related events.

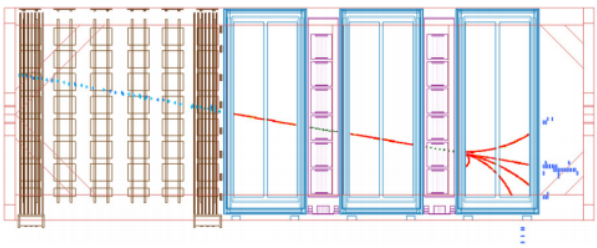

Figure 15: Typical event in the ND280 complex [4]. We can see a muon entering the tracker by the front face of the POD detector. It continues to the TPCs and FGDs region where it produces secondary particles which are stopped by the ECal detectors.

3.3.3 Technical description of the ND280's elements

UA1 Magnet

The magnet is a set of water-cooled alumium coils. The coils runs vertically and parallel to generate a magnetic fiel pointing horizontally to the right for an observer standing upstream of the detector. The magnet is surrounded by a yoke made of plates of iron.
The magnet has an external volume of 7.6 m x 5.6 m x 6.1 m and an internal one of 7.0 m x 3.5 m x 3.6 m. The coils are made of aluminium bars with 5.45 cm x 5.45 cm square cross sections within which a central hole of 23 mm allow the water to flow. The coils are split into four elements (each half has two of them). The coils are mechanically supported and electrically isolated by the yoke.

Pi-zero detectlor

The POD consiste of an interleaved arrangement of scintillator planes and fillable water target bags and brass sheet as shown on Figure **??**. The water bags can be filled or emptied to enable subtraction method to deterine the water targets cross-sections. The scintillators bars allow reconstruction of charged particle tracks.
One can count 40 scintillator modules in the POD with each module composed of two perpendicular arrays of triangular scintillator bars. Each modules contains 134 vertical bars of 2200 mm long and 126 horizontal bars of 2340 mm long. Each bar has an WLS fiber in it connected to an MPPC which make a total of 10400 readable channels.

Time projection chamber

The TPCs are made of an inner box containing an argon-based drift gas which is inside an outer box holding CO_2 as an insulating gas. The inner and outer walls are made of composite panels which, along with the central cathode, create an uniform electric field. The field is roughly aligned with the magnetic fiel provided by the UA1 magnet. The outer dimension of a TPC are 2.3 m x 2.4 m x 1.0 m. Design of a TPC is shown in Figure 16.
When a charged particle pass through a TPC, it produces ionization (electron) in the gas that go away from the cathode toward one of the readout plane. The electrons are then multiplied and sampled with bulk micromegas detectors[17] with a 7.0 mm x 9.0 mm anode pad segmentation. Combining both the pattern of the signals in the pad plane and the arrival time of the signal to give a 3D image of the track of the charged particle. We estime the point spatial resolution by comparing the transverse coordinate resulting from the global track with the informations given by a single column of pads. For now, we have a 0.7 mm

[17] a bulk micromegas detectors is blblbla reference

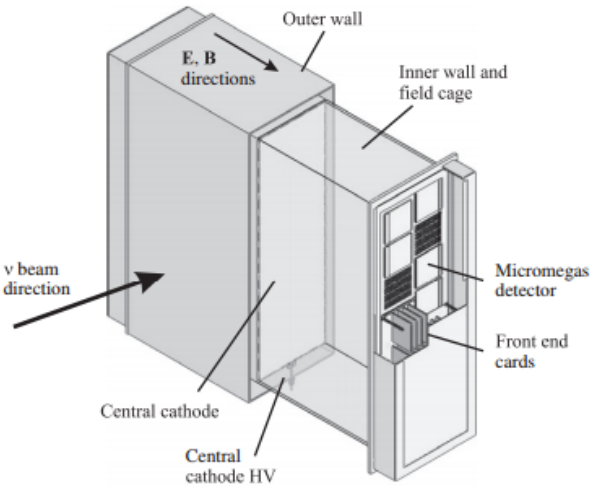

Figure 16: Cut of the TPC design [4]

resolution per column which is according to expectations and sufficient to fulfill the purpose of the TPC.

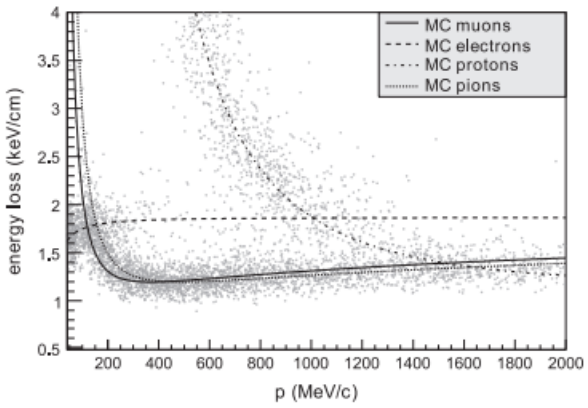

Figure 17: The curves states for the expected relationship between energy loss and momentum of positively charged particle in neutrino interactions while each point shows measurements by a single TPC[4]

Fine grained detector

The two FGD have different structure. While the first is an assembled structure of scintillator layers with each layer oriented alternatively in the x and y direction, the second alternates scintillator layer with water layer. Both FGD

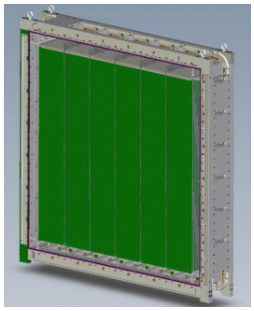

Figure 18: View of an FGD without its front. In green, one can see the scintillator modules hanging perpendicular to the direction of the neutrino beam. [4]

have outer dimensions of 2300 mm x 2400 mm x 365 mm.
The first is made of 5760 scintillators bars and has 30 layers of 192 bars each. The scintillators act as a target mass for neutrino interaction and as a detector for these same interactions. As for the other part of the detector, a WLS fiber is inserted in the bar with a photosensor connected at the end.
The second FGD still have layers of scintillator but has 6 interleaved water layer of water. Those layer are 2.5 thick and are made from a hollow structure of polycarbonate filled with water.
By comparing the interaction rates in the two FGDs, on can determine separately the cross sections on carbon and on water

Electromagnetic Calorimeter

There is 3 different type of module composing the Ecal as one can see in Figure 14. First, there are 6 Barrel-ECal modules which surround the tracker volume on its four side. Then we have one downstream module (Ds-ECal) which covers the downstream exit of the tracker volume. Finally there are 6 POD-ECal modules surrounding the POD on its four side.
Each module is composed of consecutive scintillator bars layers glued to a sheet of lead converter. All scintillator bars have a 4.0 cm x 1.0 cm cross section an have a WLS fiber inside them. An example of module can be seen in Figure 19.

Side Muon Range Detector

The SMRD fill some of the gaps between the iron plates of the UA1 yoke. These gaps are instrumented by plastic scintillator planes with WLS fiber running through them. The SMRD count a total of 440 scintillator modules.

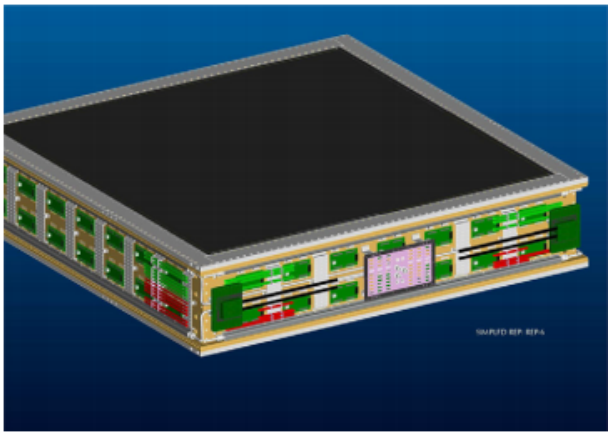

Figure 19: External view of one ECal module. The module is sandwhiched between to carbon fiber plate (in black). The scintillator bars run horizontally inside the module [4].

3.3.4 ND280 problematic

The goal of the near detectors is to provide enough - and good - data to make prediction for the signal event at the far detector. One can see a list of uncertainties for the T2K experiment on Table 3. Looking at this table, we figure out that the largest uncertainty comes from the non-canceling cross section.

Table 3: Uncertainties for predicted number of signal events for different oscillation modes [12].

Systematics	$\nu_\mu \rightarrow \nu_e$	$\nu_\mu \rightarrow \nu_\mu$	$\overline{\nu_\mu} \rightarrow \overline{\nu_\mu}$
Flux & Cross-section	3.1	2.7	3.4
Non-canceling Cross-sectio	4.7	5.0	10.0
Super-K detector etc.	2.4	3.0	2.1
FSI + SI	2.7	4.0	3.8
Total	6.8	7.7	11.6

As described above, ND280 is trying to measure cross-section on water and on carbon. The measure of the cross-section on water is crucial because the far detector is also full of water and ideally the neutrino interactions studied in the near detector would be the same as in the far detector. However, the analysis of the interaction in water is "parasited" by the multiple interactions in the other layers which must be subtracted.
To improve our knowledge of these cross-section, a new experiment has been approved : WAGASCI.

3.4 WAGASCI

WAGASCI stands for WAter Grid And SCIntillator detector [12, 13]. Its objective is to complete the ND280 complex at the T2K experiment. Indeed, for a precise study of neutrino oscillation, it is crucial to have a good understanding of neutrino interactions in nucleus[18]. As explained in the previous section, the complexity of the ND280 detectors makes it difficult to calculate precisely the cross-section in water and in carbon. This leads to uncertainty on the neutrino cross section that is one of the largest systematic error in the analysis.
The WAGASCI experiment was proposed in order to reduce these uncertainties. It would take place in the ND280 as shown in Figure 20. Its goals are to measure H_2O to CH CC cross-section with good accuracy and measure CC cross-section for H_2O and CH individually.

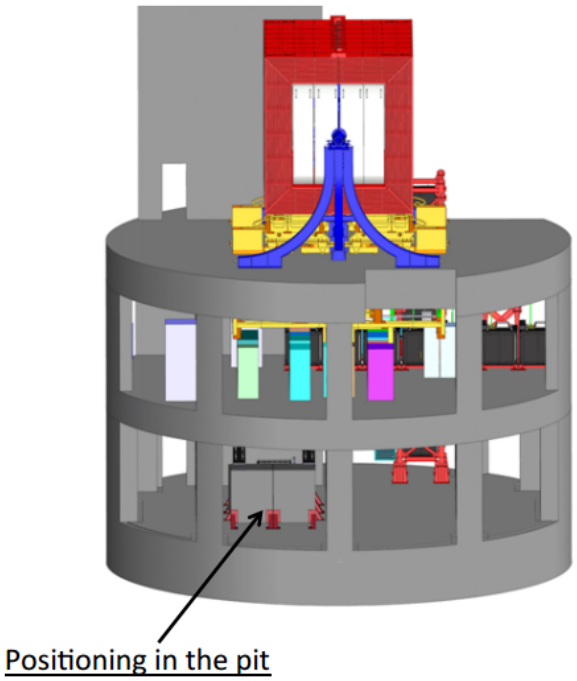

Figure 20: Localisation of the WAGASCI experiment inside the ND280 pit [15].

The WAGASCI detector is effectively a central neutrino interaction target, a grid of scintillators filled by water (H_20) and/or hydrocarbon (CH), surrounded by 2 side muon range detector (SMRD) and one downstream muon range detector. This last downstream muon range detector was originally quite similar

[18] particularly in water because the far detector is a water cherenkov detector.

to the SMRDs, but now it has become the BabyMIND detector[19]. An overview of the WAGASCI detector can be seen in Figure 21.

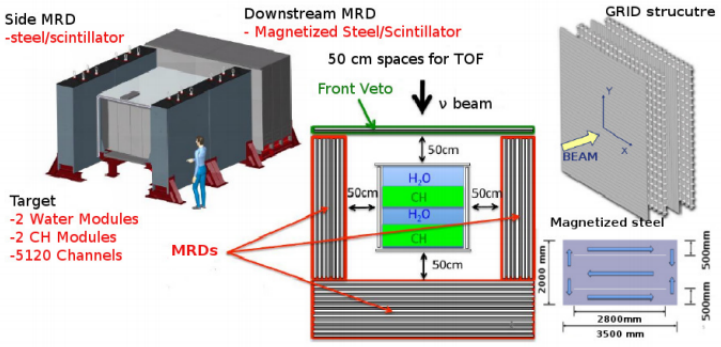

Figure 21: In the center of the detector lies the neutrino interaction target. One can see on the top view four different modules filled either by water or by hydrocarbon. On the right, one can have a glimpse of the grid structure of the neutrino target. On the side, there are the MRDs which have an alternate structure of scintillator layer and iron layer. Eventually, the downstream MRD gives a preview of the future BabyMIND structure with its magnetized plates of steel [12].

[19]the BabyMIND detector will be described and discuss in detail in the next section. We won't speak about it here

The Neutrino Target

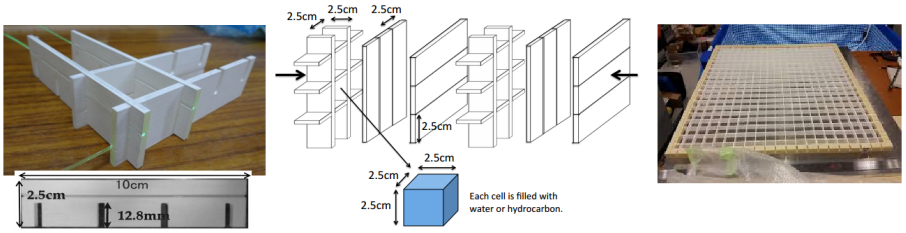

Figure 22: On the right is the photo of an unique cell. One can see the detail of the scintillator bar and the little slots that are all along the bar. In the center is a sketch of the final assembly. Eventually, there is a photo of an assembled grid on the left[13, 14, 15].

The neutrino target interaction is a grid built from scintillators bars. These bars make 1000 mm x 25 mm x 3 mm, they are painted with a TiO_2 reflector. Inside each bar, there is a WLS fiber which will be connected to an MPPC. Full assembled thes give a module of 1 m x 1 m of surface perpendicular to the beam. The cells formed by the grid are destined to be filled by water or hydrocarbon. With the 4 modules assembled, the target has a size of 1m x 1m x 2m. The details of the assembly of the grid is shown on Figure 22.

When a neutrino interacts in the target, it will produce a charged particle whose path will be registred by the grid. Afterwards, the charged particle will reach the side MRDs (or the downstream MRD, unless stopped elsewhere). That is the MRDs which will measure the momenta of the produced particle and, in the case of the dowstream MRD (BabyMIND) identificates its charge.

The Side Muon Range Detector

The MRDs will be simple structure of alternating iron layers and scintillator layers. The plastic scintillator bars will be the same than the one of the target (excepting the slots). Here, they will also be connected to MPPCs. These MPPCs are from a new generation of Hamamatsu's photosensor. They have a low dark noise rate, a wider range of operation over voltage[20], a low rate of after pulse and a low crosstalk between the pixels. The scintillators were tested in order to verify their ability to detect with high efficiency the particles. They were tested with a positron beam of 600 MeV. The bars registered an average light yield about 10 to 18 photo-electron and an efficiency >99% for the whole region of scintillator for a threshold of 1.5 photo-electron.
In order to reconstruct the tracks the time of flight information between the target and the MRDs willbe used. However, the MRDs won't be able to distinguish positive from negative particle.

Beam in WAGASCI

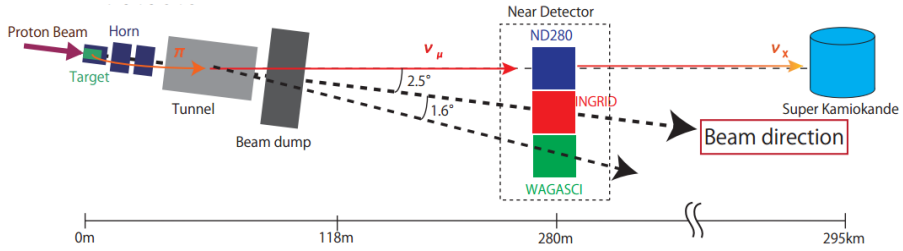

Figure 23: Direction of the Neutrino Beam at J-PARC and relative position of WAGASCI. The INGRID detector is centered on-axis, but it covers a larger area since the WAGASCI detector is located behind one of its module [16].

WAGASCI takes place in the third level of the ND280 pit. For this reason, it is necessarly off-axis. It is actually 1.6^0 off-axis (Figure 23). However, this angle, according to the simulations, should give a ν flux similar to the one of ND280 as shown in Figure 24

Expectations

The goal of WAGASCI is to reduce the systematical errors discussed in Table 3 to 3%. For now, the expected performance of WAGASCI was studied through simulations :JNUBEAM for the neutrino flux, NEUT for neutrino interactions inside the detector. GEANT4 was used to implement the propagation of secondary particles through the detector. A track is identified by a signal in a cell of the target and entering one of the MRDs. The MRDs are then used to

[20] around 4V. It allows to increase the efficiency

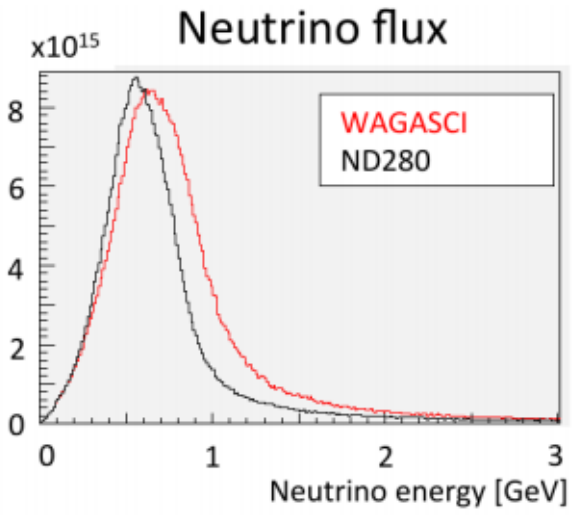

Figure 24: The expected value of the ν flux at WAGASCI is in red. It peaks at 0.7 GeV, which is quite close the ν flux at ND280 in black [12].

identify a long muon track. The tracks crossing the target and the MRDs are required to stop in the detector. For 10^{21} simulated protons on target (POT), they expect to detect $3 \cdot 10^3$ events in hydrocarbon and $2.5 \cdot 10^3$ in water. Among these events, it is expected to have 91.0% of charged current events in hydrocarbon and 75.5% for water.
At the time of the publication of this text, a prototype of WAGASCI's target has been delivered. It makes 125 cm x 125 cm x 46 cm for a total mass of 1.2 kton. The final WAGASCI detector is expected to reach the 3% uncertainty for 10^{20} POT in ν mode and 5% uncertainty for $2 \cdot 10^{20}$ in the $\overline{\nu}$ mode. It should be tested during the fall of 2016. It will be installed in front the central INGRID module. The construction of the actual WAGASCI should be begun in the same time.

4 The Baby MIND detector

4.1 Goals

The Baby MIND takes its name from Magnetized Iron Neutrino Detector [17]. This kind of detector was already used in the past years. Indeed, their structure allows them to characterized charged particle by their charge-sign and their momenta. That's why they naturally take place in neutrino experiment. Indeed, the aim of the BabyMIND project is to measure muon charge with high charge identification efficiencies. This information is really important because it gives indirectly information of the neutrino beam itself : momenta, type of flavour and therefore information on the contamination of a neutrino beam.
The Baby MIND project has its roots in prototyping activities funded by the AIDA project. Several components and ideas were carried over from the AIDA project. Eventually, the project leads to the realisation of the Totally Active Scintillator Detectors (TASD) which consist of several layer of grid of scintillator bars destined to be immersed in large volume magnetic field. The scintillating material and the electronics of the TASD was the same than for the MIND. That's why one can see the TASD as a precursor of the MIND. The AIDA project built a TASD prototype who was widely utilised to test the material (scintillators and photosensors) as well as the electronics, all things which are destined to be re-use for the Baby MIND. For now, the final test of the TASD took place in 2 beam test in the CERN facility during the summer 2016.
The Baby MIND consists of a sandwich structure of layer of magnetized iron alterate with scintillator grid. Because of his size and his function, the Baby MIND was well suited for the WAGASCI experiment. It replaced the original downstream Muon Range Detector in the WAGASCI project [21]. For now, the Baby MIND is still under developpement.

The Baby MIND was approved by the CERN Research Board in December 2015 as NP5[22]. It is supposed to be operating at J-PARC as the downstream MRD of WAGASCI for the fourth quarter of 2017. For now, the first prototype of the detector is still in construction. The first magnetized iron plate is already done, but the first scintillator module has not been released yet. There is still some scintillator bars in production, and electronics tests are still in progress as well for simulation.
Once all these elements assembled, the Baby MIND will look like the projection of Figure 25. As in the case of the TASD modules developed for AIDA, all Baby MIND scintillator modules are independent, which allows a lot of different possible configuration. The final configuration, for now, is shown on Figure 26.

[21] see section 3.4
[22] stands for Neutrino Platform experiment number 5

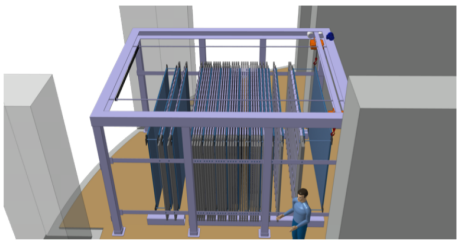

Figure 25: Baby MIND at WAGASCI[17].

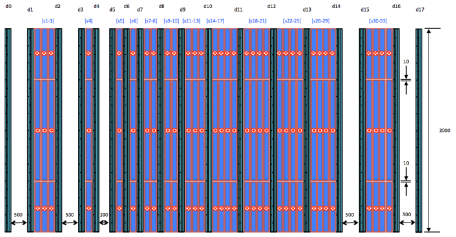

Figure 26: Baby MIND final layout. Scintillator modules are display in aqua marine while the iron plates are in blue. The direction of the magnetic field running into them is given in red.

4.2 Magnet

There are 33 steel plates composing the magnetized part of the Baby MIND. There are 2 horizontal slots in each plate. A conducting material run like a coil around the plate, passing through the slots. When an electric current runs into the coil, a magnetic fiel is *de facto* induced inside the plate. Those plates were designed and built at the CERN.
In Figure 26, one can already see there is 3 distinguished magnetized region in one plate. There is several reason why such a design was chosen. First, the plate could have been surrounded by a single coil surrounding the entire plate. However, this design would have induced big power dissipation and a stray field outside the plates. A magnetic field outside the plate could have been a serious problem for the detector, as it could have damaged the electronics and it would have implied some supplementary security issues. For these reasons, the 1-coil design was abandonned. So, why not 2-coils and only 1 slot instead of the final 3 coils/2 slots design ? In fact, if one wants to have the magnetic flux completely inside the steel, it requires (looking at Figure 27) that the cross-section between A and A' is the same than the cross-section with B and B'. So, if there was only 1 slot, the A-A' distance would have been bigger and so would have the distance B-B', resulting in a smaller tracking region[23].

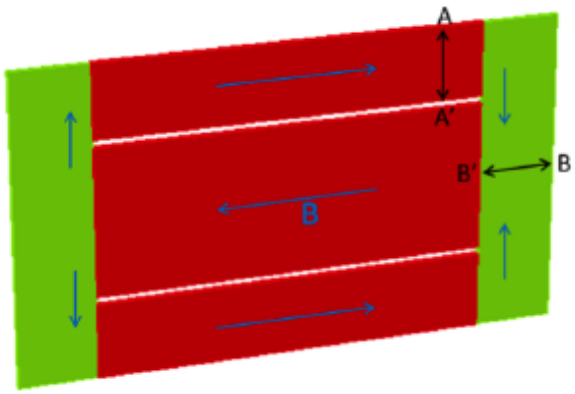

Figure 27: Final design of the magnet. The green is the steel, surrounding by the coils in red that induce the magnetic field in blue[17].

The coils consist of aluminium fine bars, bent and inserted in ans insulating sheath. It would have been possible, and maybe more practical, to wind the coils on separate plates, but it would have created discontinuity in the flux, which is why this solution was not kept. 1 cm space is allowed for the total coil[24], it naturally implies a minimal 1 cm gap between the plate and another piece

[23] we consider the tracking region the one where the magnetic field is uniform
[24] it includes 4mm aluminium,fiber glass sheath and air

of the Baby MIND. Taking advantage of this gap, additional 1 cm thick plates were added on the green region of Figure 27 on both side. This extra-thickness extend the cross-section between B and B' and then allow us to expand the A-A' distance. In theory, these extra plates could be located only neaer the edges of the slots. However, it has been decided to extend them to the full height to avoid possible losses of the flux.
Finally, the steel plates make 3.5 m width x 2.0 m height x 0.03 m thickness with a tracking region of 2.8 m x 2.0 m. This solution is independant of the choice of the material of the plate and of the coil winding technique.
However, the choice of the material affects the operating current. After some tests and measurement, Armco was retained as material for the plate, offering a good price-performance ratio. To operate the magnet with a uniform 1.5 T field, it would require 130-140 A for 1.5 T (for 33 magnet modules and I=150 A, P=12.4 kW) and 200 A for 2 T (for 33 magnet modules P=22.1 kW). An overview of the magnetic field is shown in Figure 28 for a 2.8 cm coil and a 1.5 T field. It shows an uniform field in the tracking region and a field entirely contained in the plate.

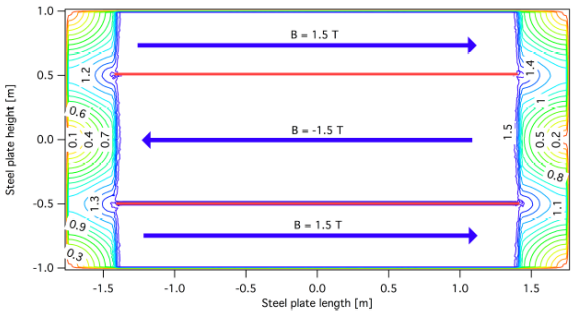

Figure 28: The field map of the final design [17].

For now, a prototype is already finished. It can be seen in Figure 29.

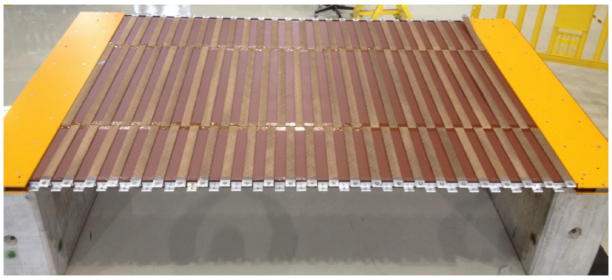

Figure 29: First prototype of the BabyMIND magnet.

At the top and at the bottom of the magnet, the aluminium sheets have to

be connected some way to be a proper coil. This "connection" system is shown on Figure 30.

Figure 30: First prototype of the BabyMIND magnet.

The "connection" system is a simple piece of aluminium. There is an idea to fix some isolation piece between the part of the coil that must not be connected but it is not accepted yet. Eventually, a plastic cover will be added on the top and bottom part of the magnet to isolate the aluminium coil from the outside. This magnet has the advantage to have a relatively low cost and can operate at low power (<200 W per module). The fact that it was desired to contain the stray field leads to some non-tracking region, but it reduces the power dissipation while leaving an acceptable tracking surface. The 1.5 T should be reachable in acceptable power and should be uniform.

4.3 Scintillators

In the developpement of the BabyMIND project, two kind of scintillator modules were designed. First, there is the TASDs modules which are composed of a single type of scintillator bars. Secondly, there is the BabyMIND modules which are composed of two types of scintillator bars : horizontal and vertical.
All the scintillator bars were produced and tested by the Institure for Nuclear Research (INR) of the Russian Academy of Sciences. All the bars were produced using the same scintillating material. These plastic bars are made of polysterene with 1.5% of paraterphenyl (PTP) and 0.01% of 1,4-bis(5-phenyloxazol-2-yl) benzene (POPOP). It is similar to the scintillator used in the SMRDs of T2K. The surface is covered by a fine layer of a chemical reflector. A 2mm deep slots has been hollowed on the full length of the bar to put a WLS fiber. These fibers are delivered by Kuraray. They are of 1mm diameter, S-type and 200 ppm. More specification on the fiber can be found in [19]. The fiber is glued to the scintillator with a silicon grease (TSF451-50M). At the end of the bars is glued a connector that aligns the fiber with a potential photosensor.
Tests has been done for the bars : TASD scintillator bars and the horizontal bars of BabyMIND were tested in Russia while the vertical bars were tested during the July 2016 Beam test. Both timing and light yield were tested. Results can be seen in Table 4.

Table 4: Typical light yield for the different types of scintillator bars. The light yield is the sum of both ends.

Type of bar	Typical Light-Yield (p.e./MIP)	Typical particles
TASD	100	Cosmic μ
Horizontal	60	Cosmic μ
Vertical	35	Beam of 10 Gev/c μ

The typical light yield of the bars is shown on Figure 31.

Ending the scintillator bar lies a crucial piece : the connector. This piece must transmit the signal with the best efficiency and quality possible. As for the scintillators, there were produced by the INR inspired by the connectors used in the MICE EMR experiment. Finally, one can see a complete scintillator bar on Figure 32:

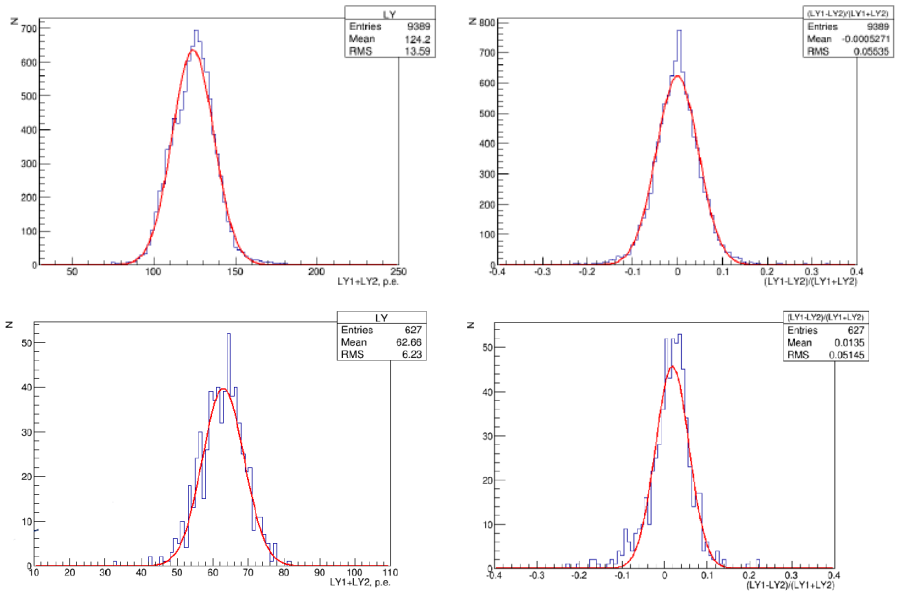

Figure 31: On the first row is the results for the TASD scintillator bars. On top left is the Light Yield (both end added) and top right is the asymetry of the light yield ($\frac{LY1-LY2}{LY1}$)[17]. The second row is the same result for the horizontal bars.

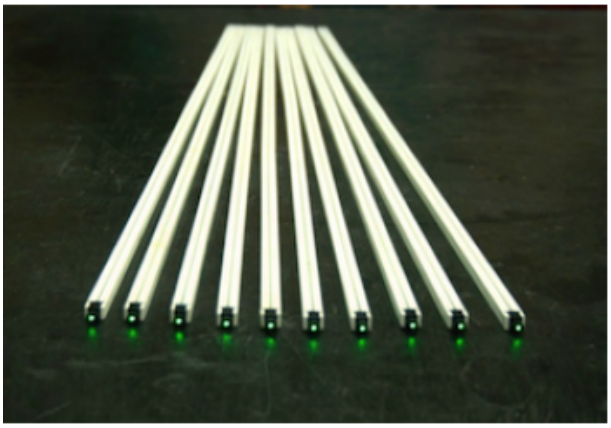

Figure 32: Example of the scintillator bars used for the TASD modules [17].

4.4 Photosensors

The photosensors chosen for the full Baby MIND project were one of the new generation of photosensors : the *Hamamatsu MPPC S12571-025C* whose caracteristics are given in Table 5. MPPC stands for Multi-Pixel Photon Counter and are a type of Silicone Photo-Multiplier (SiPM). It consists of a matrix of cells detecting light through Avalanche-PhotoDiods (APD) in Geiger mode. In fact, even if a single photon touch a cell, the APD will amplify the signal and produce a large amount of electrons. The main problem with these photosensors is a possible crosstalk between the cells and the afterpulse of the signal that can induce some errors. The photosensors chosen for the project have a low afterpulse and provide lower crosstalk and lower dark count than their predecessors. Therefore, they are suited for precision measurement, that requires low noise characteristics [18].

Table 5: Hamamatsu MPPC Characteristics

Surface	Cell size	Pixels	Operating voltage	PDE[25]	Gain	Dark Counts
1mm x 1mm	25μm	1600	67.5 V	35%	$5 \cdot 10^5$	100 kcps typ.

There was several constraints for the choice of the photosensor. In this case, the constraints came mostly from the electronics. The photosensors should be adapted to the caracteristics of the readout chip. The resolution of the MPPC must be sufficient to perform calibration in a peak-to-peak way. This requires a low cross-talk as well as a low noise level. Furthermore, the photosensor should be adapted to the WLS fiber. This put a constraint on the photosensor active area which must matched to the light coming from the fiber. Tests showed that 90% of the light is transmitted down to the fiber core. The fiber making 1mm diameter, these results allow to use the 1mm x 1mm SiPM. Those were $\frac{2}{3}$ the price of their bigger cousins of 1.3mm x 1.3mm which were the other possibility so the cheaper ones were naturally chosen. Because of the really close size of the MPPC and the fiber, the connection between the fiber and the photosensor was a crucial point that lead to the actual design of the connectors.

4.5 Electronics

4.5.1 Citiroc Chip Description

The readout system of the Baby MIND detector is based on a new Front End Board using a CITIROC readout chip [17, 20]. CITIROC is chip developped by Omega for the readout of SiPM detectors. Being a new product, there was no real documentation on the CITIROC, that is why a huge work was to understand its running and fonctionalities. For this purpose, the CITIROC was delivered with an Evaluation Board allowing simple readout of the signal and monitoring by a LabView software. In parallel to the tests on the evaluation board, a new FEB was in developpement at the UNIversity of GEneva (UNIGE) under the direction of Y. Favre. The first version of the new FEB and of the software monitoring it were released in spring 2016. Some modifications were done in order to be ready for the 2 beam test of the summer 2016. The main goal of these beam tests was to test the electronics and the new FEB in real data acquisition conditions.

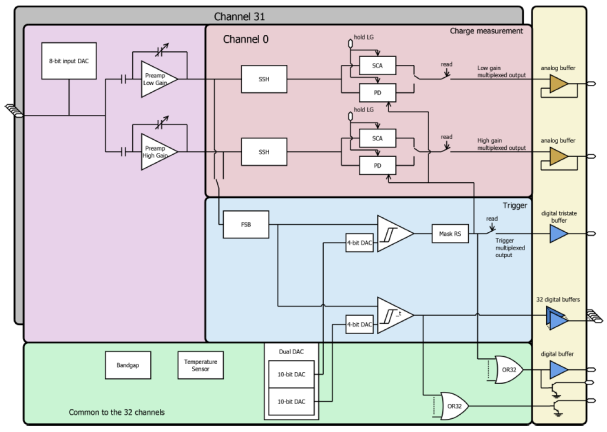

Figure 33: Architecture of the CITIROC chip [21].

The analog characteriscs and the electronic chain which will be describe can be observed in Figure 33. A summary of the different characteristics is displayed on Table 6.
The CITIROC possess 32 fully analogue chanels operating at low power. First, a fine tuning of the applied voltage on each SiPM can be performed using an 8-bit Digital-to-Analog (DAC). The range of the tuning goes from 0 to 4.5 V. The analogue core is sensitive to positive SiPM only.
For each channel, there is 2 parallel AC coupled voltage preamplifiers (the Low Gain LG and the High Gain HG). The gain is related to the value of a small capacitance. 6 bits tuned from 0 to 1575 fF with steps of 25 fF the capacitance individually for the both capacitance. The gain is given by C_{in}/C_f, with

$C_{in} = 15pF$ for HG and $C_{in} = 1.5pF$ for LG[26]. The capacitances ensure the read out of the charge from 160 fC to 320 pC, which corresponds to 1 to 2000 photo-electrons with a Gain of 10^6 (with a p.e. over noise ratio of 10). Then, From this points the two electronics chains of LG and HG follow a similar process.
After the LG/HG, there is a tunable shaper (SSH for slow shaper) which are used to reduce the noise. The SSH has an adjustable time constant from 12.5 ns to 87,5 ns. Varying the time constant allow to reduce the noise depending of the application.
The SSH is followed by 2 "trac-and-hold" device which will try to capture and hold the maximum value of the signal. This is this hold value that the user will read at the end. The first system is a Switched Capacitor Array (SCA) whose time constant OR32 can be set manually to fix the final value. The second one is an active peak detector (PD) which will detect detect automatically the culminant point of the signal to hold.
There is a third electronic chain whose purpose is to parametrize the trigger. This chain uses a bipolar fast shaper (FSB). It has a 15 ns fixed shaping time. The FSB can be derived from the HG or the LG chain. The FSB is followed by 2 discriminators. There is also a 10-bits DAC common to the 32 channels which sets the programmable threshold to the discriminators. This value can be tuned individually by a 4-bit DAC. The first of the two discriminators will provide the trigger which will be common for all channel (it can be individually mask). The second discriminator gives a different value for each channel and provide an event time information.

Table 6: Main Characteristics of the CITIROC Chip [22].

Technology :	Austria-Micro-System (AMS) SiGe 0.35 μm
Dimensions :	4.1mm x 4.1mm
Power supply :	4.5 V
Comsumption :	5 mW per channel 96 mW all outputs on
Outputs :	32 trigger outputs 1 multiplexed charge output 1 ASIC trigger output (Trigger OR)
Internal Programmable Features :	32 HV adjustments (32x8bits) Trigger Threshold Adjustment (1 for all channels)(10 bits) Gain tuning (for each channel) 32 Trigger masks Channel by Channel output enable

[26] C_{in} is a capacitance at the entry of the preamplifier, C_f is the tunable capacitance in parallel with the preamplifier

4.5.2 Electronic chain

Figure 34 shows the electronic chain chain of the experiment. This system is base on the MICE-EMR one.
However, the electronic chain of Figure 34 is not the final one. It is still under discussion and its final form has not been decided yet. The chain of figure 34 is the one which was presented during the Collaboration Meeting of BabyMIND in April 2016.

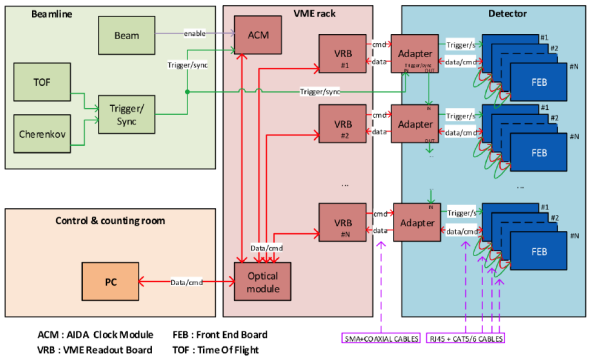

Figure 34: Electronic chain [17].

4.5.3 Citiroc Evaluation Board

The Evaluation Board was delivered with the CITIROC. It is designed to monitor and access simply the different functionalities of the chip. The evaluation board was used on the TASD modules until april 2016. A LabView program coming along with the chip too was monitoring the slow controls of the chip. The connection between the board and the computer was in USB2. A lot of different tests were done with the evaluation board. Although the design of the new Front End Board was fixed in spring 2015, its development has taken a whole year. During this period, it was the evaluation board who helped characterizing the chip.
An image of the evaluation board as well as a more specific description can be seen in Figure 35.

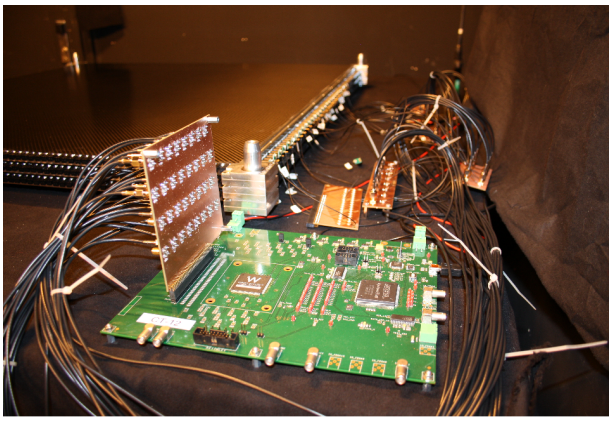

Figure 35: The Evaluation Board used in a typical test. In the back lie 3 TASDs modules. On left side of the board a rectangular card is connected to the 32 channels. This card was built at UNIGE to allow an easier way of connecting the channel to the MPPCs. In the center, one can see the CITIROC chip with its "W" written on it. Right from it is the FPGA. There is at the extreme right of the board an USB cable going to the computer in the room next door.

4.5.4 Citiroc Geneva University's Front End Board

The New FEB contains 3 CITIROC chips for a total of 96 readable channels. Furthermore, it is now connected through USB3 allowing a huge improvment in the data acquisition. The FEB were tested during the spring and mainly during the beam test of summer 2016. They are destined to be the final readout support for the BabyMIND detector. This time, a software was developped by UNIGE to monitor the boards.

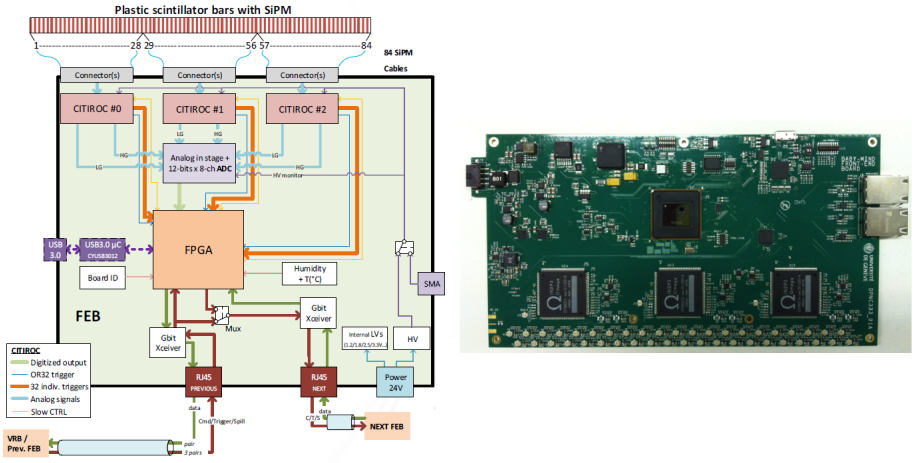

Figure 36: On the left is the scheme of the FEB. On the right is the first prototype of the FEB. In fact, there was 3 little boards glued right next to the CITIROC. This adding was to solve a big noise interference on the board.

4.5.5 FPGA Firmware

The FPGA firmware is shown in Figure 37. In spring 2016, the analog, slow control, data link communication blocks and the USB interface were fully tested on hardware. The timing and readout blocks were tested for the beam test.

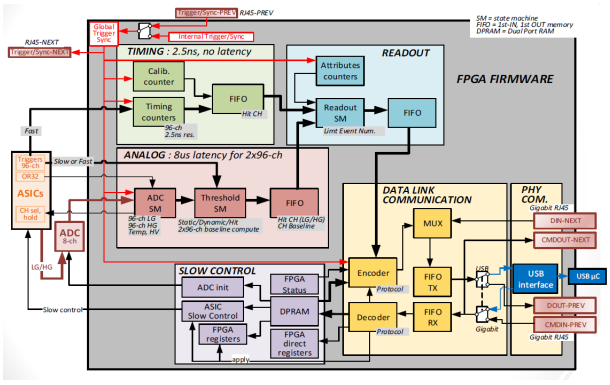

Figure 37:

4.6 AIDA TASD Modules

The full detector is composed of 50 TASD modules. A TASD module consists of 2 planes of scintillator bars (X and Y), hold fixed on an aluminium structure and protected on its top and bottom face by a fine sheet of carbon. All parts of the module are glued together. All scintillator bars are embed with a WLS fiber and can be read out at both end by an MPPC. The acquisition of data is monitored by a Front-End Board developped by the University of Geneva.
There are 84 scintillator bars per plane, which made a total of 168 scintillator bars for a module. Each bar has the same dimension of 1.0 cm x 0.7 cm x 90 cm (width, height and length respectively). The all 50 modules compactly assembled make 1 m^3 in volume. Even in this simple configuration it can identify pions from muons at low momenta (280 MeV), pions having a range of 60 cm in plastic while muons go to 72 cm. Having each module independant allow to insert other components inbetween (from active detectors until layer of passive material like iron). One can see how a TASD module has been assemble in Figure 38

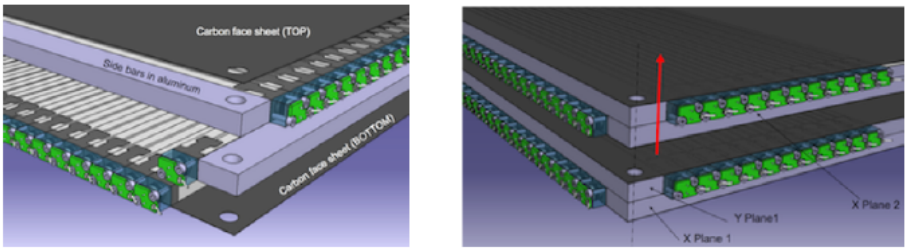

Figure 38: The figures show how the X and Y planes of scintillator bars are fixed to their aluminium structure and their sheet of carbon.

The scintillating material, MPPCs and electronics of the TASDs are destined to be re-used for the Baby MIND project. That's why a lot of test have been done on the TASD, finishing by a beam test at CERN whose purpose was to test the electronics[27] for the future Baby MIND. However, the TASDs modules are "finite product" and they can be used in other experiments.

[27] as they share their electronics, the description will be given in section 4.5

4.7 Baby MIND Modules

The design of the Baby MIND module is different from the TASD. First, there is two kind of scintillator bars. If the horizontal ones, apart from the dimensions, look like the TASD ones, the vertical ones are quite different because they have the two end, and so the two MPPC, on the same side (see Figure 39). Furthermore, having some issues with gluing the scintillators, there will be no use of glue anymore. The bars will hold thanks to pressure and some piece of yet undefined material.

Figure 39: The left shows the vertical bars. The right shows the horizontal ones.

The module consist of two half. One half has 47 (48 for the other) horizontal bars of 3000 mm x 31 mm x 7.5 mm and 8 vertical bars of 1950 mm x 210 mm x 7 mm. The bars are surrounded by a metallic structure. The vertical bar are in the exterior of the module, and the horizontal in the interior. A protection sheet will be certainly added to cover the vertical bars. When the 2 half are put together, no bar is aligned with its homologue. In fact, as their must be some material between the bar to hold them together and avoid them to bend, there is some gap between them. That's why each bar from a half is shifted compared to its "sister" on the other half (see Figures 40 and 41). This way, the scintillator bars cover all the plane.

For now, the horizontal bars have not yet been all delivered to the CERN. A first module of the Baby MIND should be finished for the end of september. The whole detector (magnet + scintillator) sould be finished for the second quarter of 2017 [28]

[28] See the schedule of BabyMIND in

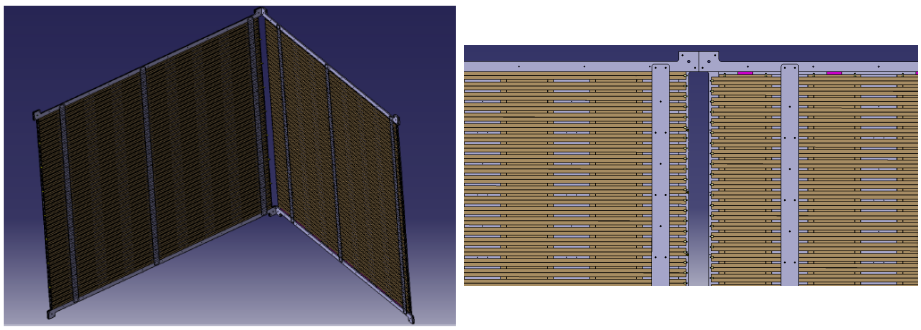

Figure 40: The left shows the vertical bars. The right shows the horizontal ones.

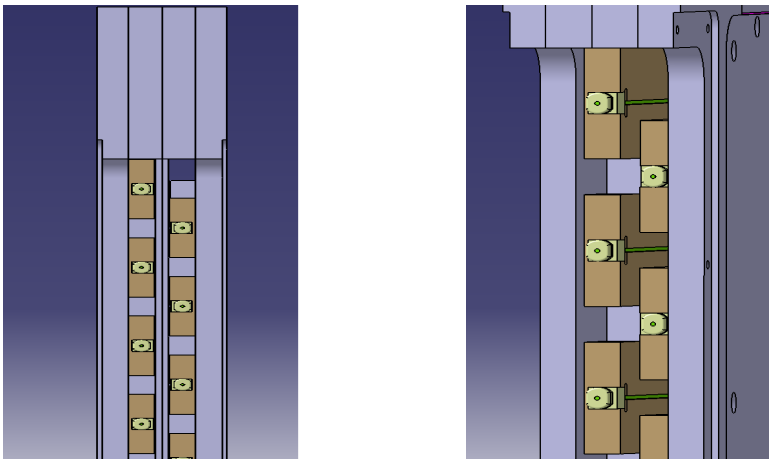

Figure 41: This side view of the horizontal bars illustrates thw shifted alignement of the scintillator. In this arrangement, the bars will cover all the plane.

5 Experiments

5.1 Calibration

5.1.1 Citiroc Evaluation Board

Doing a Calibration, we are interested by the number of photo-electrons (p.e.) detected by the MPPC. However, we won't see directly this value when running in a beam test condition or in cosmic rays. In fact, the calibration procedure uses the dark count. The dark counts is the number of pulses registered by the MPPC in the absence of light. It is an intrisic noise generated by free carriers unrelated to the incidence of photons on the SiPM. That can be also done at low treshold value. In the resulting histogram of a dark count acquisition, the p.e. reveal themselves as discrete peaks. The fact is that the difference between the peaks gives us the ADC/p.e. ratio. Once we have this ratio, we can convert the ADC values we obtain in operating mode[29] in p.e.
Several calibration tests have been done in order to characterize the chip and understand its working. Here, we will give an overview of the most important calibration we conducted. All the calibrations were done on some TASD modules in a dark room at CERN. There was generally 3 TASDs module stacked. 32 MPPC were connected to different bars of the TASD to have X and Y bar connected and even some Z coincidence. A little PCB is connected to the MPPC. A coaxial cable of 0.4m connects then the PBC to a card, where another cable of 1m relays the signal to the evaluation board. A USB2 cable connects the board to the PC next door through the wall.

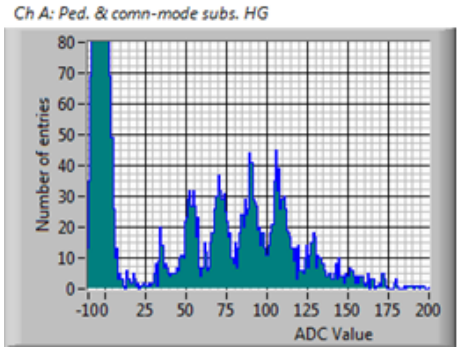

Figure 42: The picture show a typical calibration in High Gain. For this one, the High Gain was set at 8 (which represent a real Gain of $\frac{1500[fF]}{8 \cdot 25[fF]} = 7.5$). The first and huge peak is the pedestal of the signal, it is not a p.e. peak. In this typical calibration, we change the threshold from 300 to 200 with step of 25 after 500 acquisitions. The difference between the peak can be directly calculated by the LabView program.

[29] i.e. not calibration mode

Shaper time constant and OR32 delay

At first, all calibrations were done in the SCA mode of the CITIROC chip described in section 4.5.1, so it was important to determine what was the optimal value of the OR32 delay and Shaper time constant. An exploration was done. We can see an example in Figure 43.

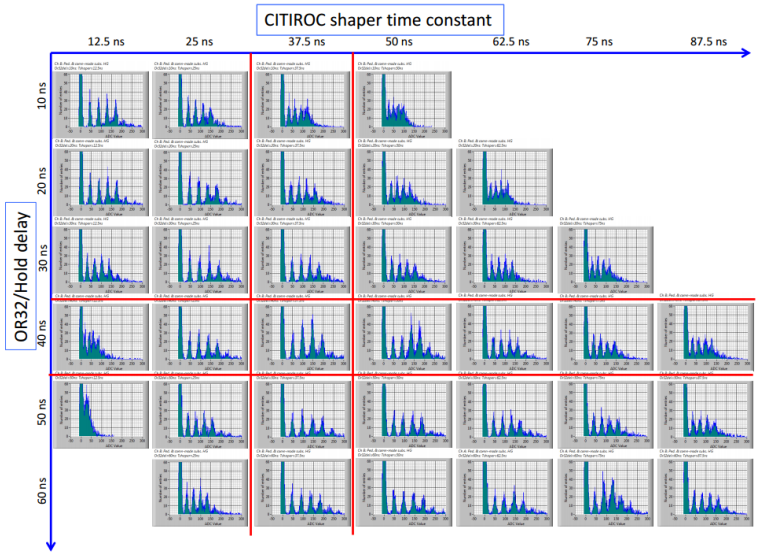

Figure 43: Calibration of the Shaper Constant

From this test, the OR32 delay was fixed to 40 ns and the Shaper time constant to 37.5 ns. It seemed to provide good resolution of the peaks. It was because the track-and-hold SCA was holding a value very close of the maximum in this settings.

Timing Studies : SCA VS Peak-detector mode

Quicly, it appeared that we needed to be sure that the settings we set in LabView were consistent with what the FPGA sets. To understand how the chip worked, we connected an oscilloscope on the evaluation board. Fixing the shaper time constant at 37.5, we varied the OR32 delay. The results are shown in Figure 44.

From the Figure, we understand the delay we choose has a huge impact on the value we read. That's why it was important to fix this OR32 with good precision. However, it was still possible to make some points having different raising time. That was not very satisfying, so we decided to check the Peak-Detector mode. The same serial of acquisition has been down and is shown on Figure 45.

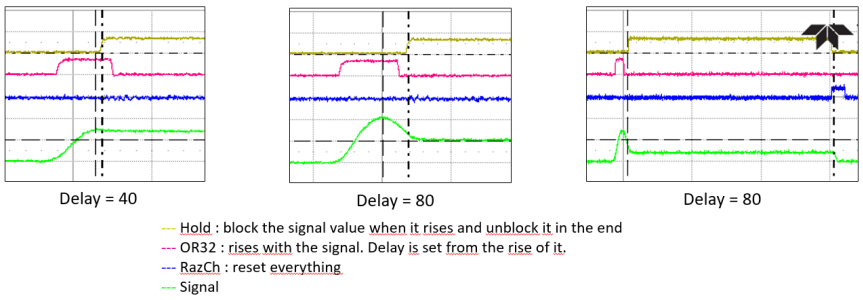

Figure 44: There are 4 distinct signals on the scope. The top one is the Hold which will hold the signal (bottom in green) when it raises. Under the Hold is the OR32 signal. The OR32 raises and after [value of delay] the Hold will raise. Under the OR32 is the RazCh. We can see on the right image that the Holds falls when the RazCh raises. It has the role of reseting the Hold and so the signal. From the image, it is easy to see that a bad setting of the OR32 induces a wrong read value.

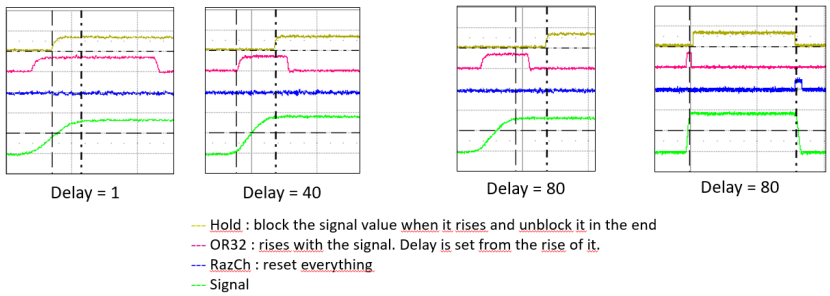

Figure 45: This is the same study than for the SCA mode in Figure 44 with the same signals displayed on the scope. However, this time the kept value is always the maximum, no matter which OR32 delay we set.

This time, the Hold doesn't seem to have an influence on the read out value anymore. The PD fix everytime the maximum value, no matter which value we set on the OR32 delay. From these results, it appears clearly that we should use the peak-detector mode instead of the SCA mode.

Gain

The Gain we set has a direct influence in the ADC/p.e. ratio which makes sense. A simple look at Figure 46 indicates clearly this dependance. Chosing the right value of Gain was difficult at this time because we were not operating with the final system and didn't know which value would be optimal. However, the Gain must be sufficient to allow us to do the calibration. That's why in

most of our tests, we set the Gain at 5.

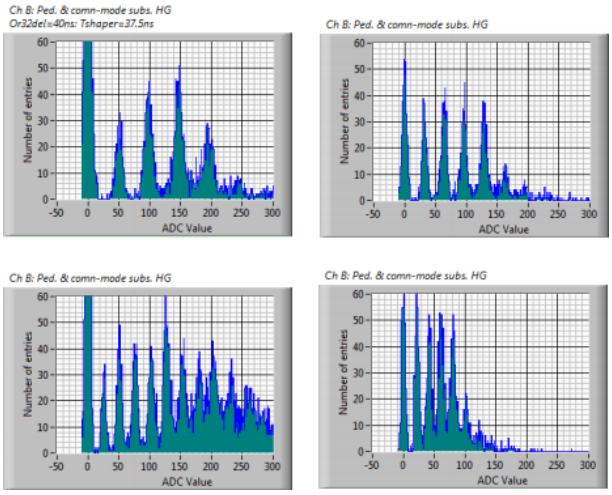

Figure 46: Top left : Gain of 60, 48.2 ADC/p.e. Top right : Gain of 15, 32.3 ADC/p.e. Bottom left : Gain of 10, 25.6 ADC/p.e. Bottom right : Gain of 7.5, 19.3 ADC/p.e.

Cabling influence

The first tests were done with short cable of 1.4m. However, we knew we would use longer cable in the final experiment. It was important to determine if the length of the cable had an influence in the ADC/p.e. ratio. For this study we compared the ADC/p.e. value using cable of 1m and cable of 4m. The results showed there was no significant difference between the two cabling.
The difference being not significative, we changed the cables for the calibration.

Other Studies

The studies were mostly done on the HG. In fact, the LG signal were too weak to distinguish the peaks and do a calibration as for the HG. The calibration of the LG is something still missing in the CITIROC characterization. However, new tests can now be performed with the new FEB.
The evaluation board has still an utility. Indeed, there is still a lot of things needing to be tested. One of the most important is the effect of the temperature on the chip. A study of this potential influence is in progress at UNIGE by S. Gleize. For this study, the evaluation board will be used, the FEB being assigned to the TASDs.

5.1.2 Citiroc Geneva University's Front End Board

With the new FEB, the calibration changed. Because of its USB3 connection, it was possible to acquire 10^6 entries in less than 10 s while it took around 10 min to acquire 5000 entries with the evaluation board. Without changing the settings in the dark room, we have conducted some calibration. This time, the board was monitored by the new software. The analysis of the data were not performed directly on the program like with LabView[30], so we used Igor. An exemple of a typical calibration is shown on Figure 47.

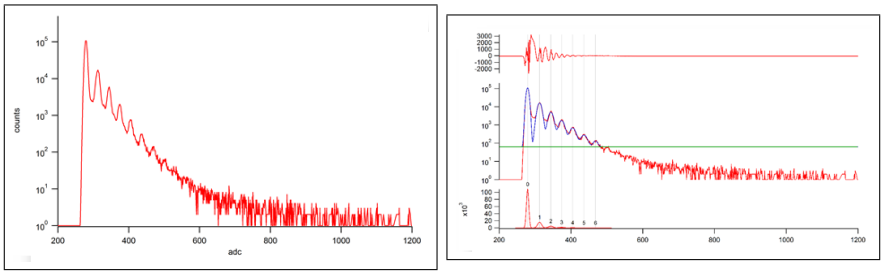

Figure 47: Left : typical calibration on one channel. Right : analysis and detection of the peaks on Igor. Looking closely, one can see that the raising of the first peak is more brutal than the rising of the others. It may be because the threshold we put is too close to the first peak.

We made a few calibrations with the new FEB. We particularly tried to investigate on the HG dependence of the ADC/p.e. ratio and the Input DAC dependance of the same ratio.

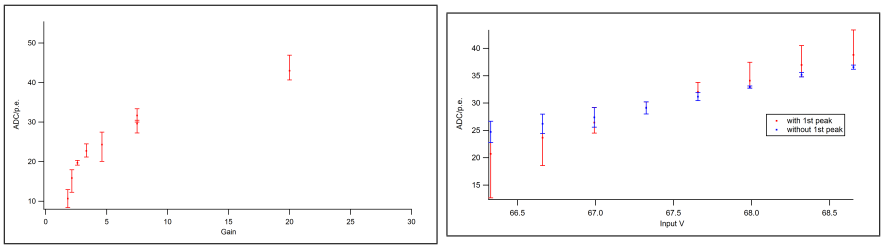

Figure 48: Left : Gain dependance. Right : Input V dependance. The error bars are not really error bars but the range of the data.

From the Gain graph on 48, we clearly see the signal reaches a saturation. This is logical because we reached the maximum values of the gain. For the Input V, we have some linear dependance to the voltage which also makes sense because the signal given by the MPPC depends of the signal we apply on it.

[30] this functionnalities has been implemented since

There is probably a saturation if we increase the voltage to the limit of the MPPC.

Another study before the beam test was on the acquisition frequency of the FEB. Making the hypothesis it was related to the Input voltage, we compared the acquisition frecquency of the board for different value of voltage. We observed that there was indeed a dependence but it was not linear but rather step-like. Looking at the results and of the evolution of the peak distribution, we think these steps corresponds at the evolution of the photo-electron peaks.

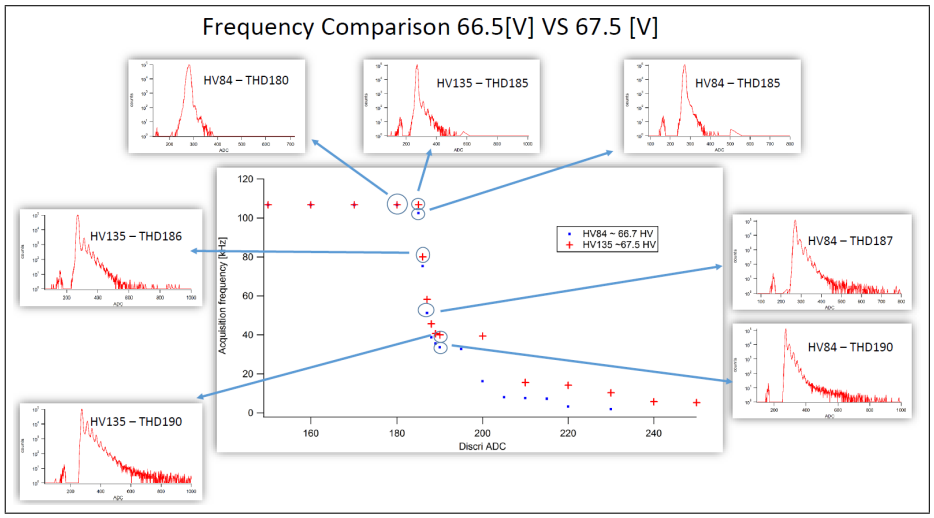

Figure 49: Study of the Acquisition Frecquency. One can see the evolution of the calibration graph for the 2 different Input voltage.

After these studies, the beam test was close and we had to focus on its preparation.

5.2 Beam test at CERN

5.2.1 Set up of the experiment

There was 2 period of beam test at CERN during summer 2016. One going from the 22 June to the 29 June and a second going from the 20 July to the 3 August. The main objective of these 2 beam test was to test the electronics in real acquisition condition. For this specific experiment, the best TASDs modules have been used. Testing the quality of the TASDs was a huge work. It consisted in send light thanks to a LED driver in every channel of every TASD module and look at the light yield[31]. Apart from this test, another selection was done on the general state of the modules. Indeed, because of a heating maladjustment, some of the modules spent a lot of time in an overheated room. This had for consequence that some of the carbon sheet peeled off. At the end, 25 TASDs modules were selected. A mechanical frame was built by UNIGE in order to fix them for the beam test.

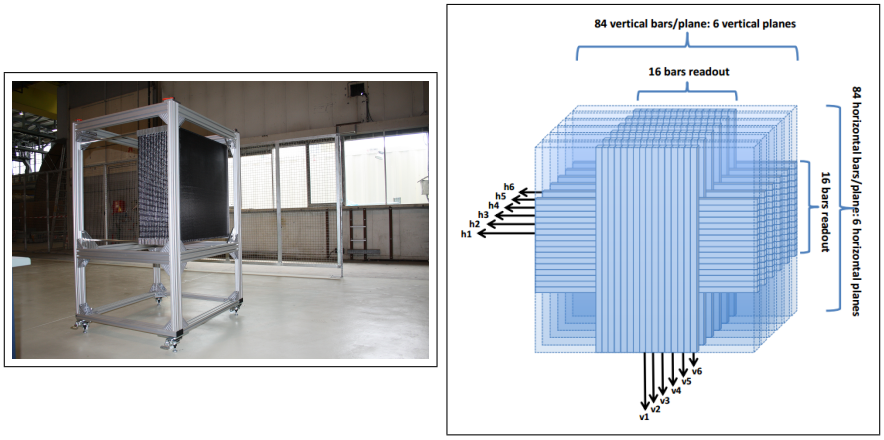

Figure 50: Left : the mechanical frame supporting the TASDs modules. Some little plate of metal were added to support the FEBs and the trigger board. Right : Scheme of the connection of the modules.

4 FEBs were available for the beam test, which make a total of 384 channels. 6 modules among the 25 were instrumented, everytime 16 bars at the center of them (so 64 channels per module). Changing the number of unconnected modules between the connected ones, the scintillating material could be use as target. A sketch of the connection is shown in right Figure 50. In this figure, one can see the presence of a trigger system. This trigger system was especially developped for the beam test. It consists of scintillator plates (the same material than the bars) located in the center of the module both in front

[31] these tests were done at CERN with an LED technology developped by the Bulgarian Academy of Science (BAS) and with the help of G. Mitev (BAS) and A. Mefodiev (INR).

and at the end of the detector. It was then connected to a trigger board that relayed the trigger signal to all the FEBs. Unfortunately, even if it was working during test, the trigger system was not adapted to the beam test and we finally used the trigger given by the beam itself.
All the FEBs were connected to a computer inside the beam zone that was itself remote controlled from the control room outside the zone. This way, it was possible to take every measure we wanted without entering the beam zone.

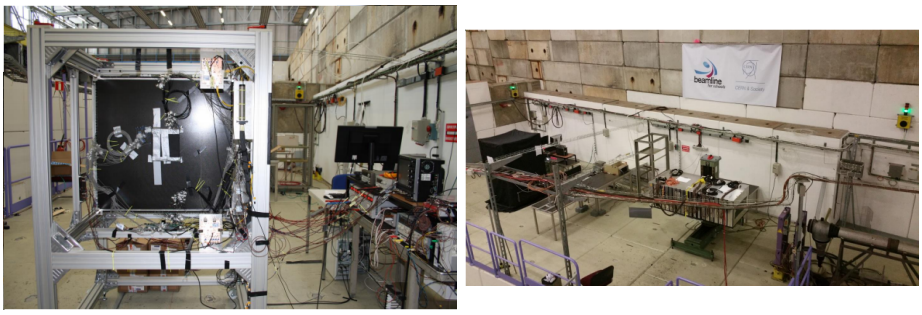

Figure 51: Left : the TASD detector in the beam zone. One can see the trigger system fixed at the center of the module. Straight down lie 2 of the FEBs, the other one are straight right to the trigger plate, hidden behind the mechanical frame. At the right of the detector are the power supplies and the computer monitoring the FEB through USB3, itself remote controlled from the control room. Right : Overview of the beam zone. The detector is on the left, it has been covered with some black covers.

5.2.2 Beam Characteristics

The beam line used for the test was the T9 beam line at CERN [23]. The tests were conducted either with hadrons or muons beams. The final beam is produced by the proton beam from the PS acceerator at cern. This proton beam then hits a target. There are different kind of target depending of the wanted final beam. The collision between the protons and the target will then produce the particle for the beam line. Among them, one find electrons, positrons, muons, pions, kaons and (anti-)protons. The particle have a momenta between 0.5 GeV and 10 GeV. The beam is delivered by burst of 0.4 seconds. The frecquency of the burst can be adjusted but is typically of 2 burst within 15 seconds. We typically had less than 10^4 hadrons per spill and $2 \cdot 10^3$ muons per spill. The beam travels around 55m before it enters the experimental area, where it can be focus depending of the wanted result.

5.2.3 First Results

The aim of the beam test was to test the electronics. This experience allowed to debug and understand a lot of issues with the FEB software or with the trigger

system. For now, the results are still in analysis, but the experiment tested the following settings :

1. Timing of signals on a given FEB
2. Synchronisation of multiple FEBs
3. DAQ protocol
4. LG and HG. We observed a linear dependance between the HG and LG, displayed in Figure
5. Shaper time constant
6. Discriminator threshold
7. Peak-detector mode versus SCA mode

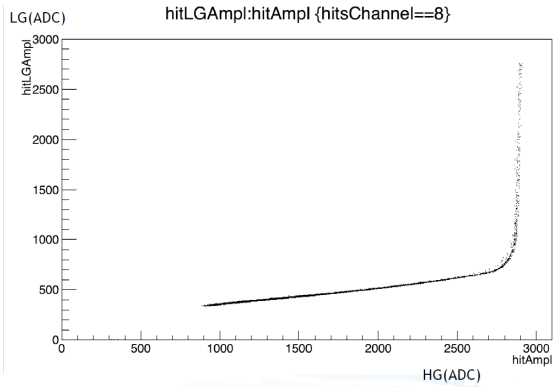

Figure 52: We observe a linear correlation between HG and LG up to the point where the HG saturates (around 2700 ADC counts). Even if the values are in ADC, this correlation is real because there is only a factor 10 between HG and LG.

On Figure 52, one can see a linear correlation between HG and LG signals. That makes sense because there is only a factor 10 between the preamplifiers. We can hope then to have a linear dependance between the 2 signals at the end. Other results are in analysis right now. One of the most interessant will be the comparison between the simulations and the experiments.

5.3 Simulations

The simulations in particle physics are very important because they provide an idea of what we can expect and mainly provide a reconstruction software which

should be able to reconstruct the position, momentum and charge identification of particles from their tracks. Furthermore, they are a good way to evaluate different detector geometries before construction.
In the Baby MIND project, there are 3 institutes doing simulations : UNIGE, INR and the University of Glasgow (UG). The INR simulations are based on the simulations of T2K near detectors simulation and use a very similar algorithm. The simulations at UNIGE are leaded by S. Parsa and are using the angle distribution of the particle after the first plates to make the charge identification and momenta reconstruction. What we will present here are the reconstruction software of UG : SaRoMan and how the work of S. Parsa on the Lever Arm helps to improved the charge identification efficiencies.

5.3.1 SaRoMan

SaRoMan stands for Simulation and Reconstruction of Muons and Neutrinos. The software was especially developped for the Baby MIND. One can find its current release at [24]. The software contains 3 different parts written in C++ :

1. **Simulation :** the simulation part uses GEANT4. GEANT4 can simulate how single particles interacts with the detector. The outputs of the simulation include the position and time of a hit on a bar, the location of this bar and the amount of energy deposited in it.

2. **Digitization :** the digitazation recreates the detector in virtual. It has to be as close as possible as reality. In this sense, it has to handle things such as the response of the electronics. The digitazation works smearing real data with different Poisson functions as well as handling events separated by a large time difference.

3. **Reconstruction :** The reconstruction takes the simulated hit data and aims to reconstructed the full track of the particle as well as its physics parameters (momentum and charge). The main problem is when there is too much hits in a bar, because it becomes complicated to associate the good hits with the good track. To solve this, the software uses a χ^2 analysis through RecPack [25] to find the best trajectory and uses various algorithms to estimate the charge and momentum using different fits.

The three parts are then handled by a python wrapper which assures a full run of the software.
The software is still in progress but shows good results. It will be used in the reconstruction of the tracks for the beam test. An example of its results is shown in Figure 53.

There is still work to do, mostly cleaning up the code for an easier utilisation and still improve the momentum estimation algorithm.

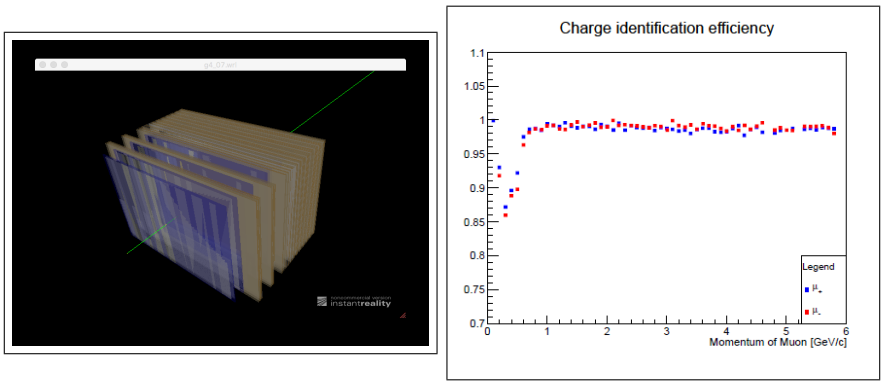

Figure 53: Left : the simulation of the final Baby MIND detector (see geometry in Figure 26) Right : The efficiency of the charge reconstruction for the Baby MIND detector. It shows a very good efficiency for muons with momenta >1 GeV.

5.3.2 Lever Arm

As one can see on figure 53, the SaRoMan algorithm has lower efficiency in the low momentum region. Improve these efficiencies at lw momentum is the main goal of the Lever-arm algorithm.
The idea is to measure the angular distribution of the tracks to procede to charge identification. The problem is the spread due to multiple scattering in the steel planes that makes the identification of the incoming muon difficult. However, by introducing gaps before and after a stack of magnetic modules and adjusting their length and the thickness of the magnetic modules, one can increase the angular resolution. The modularity of the Baby MIND detector allows us to optimize the detector performance using the Lever-arm.

First, the angular resolution depends on the hit resolution and the separation between the detector planes, so it was important to look for the best layout. For example, one has a 1.2^0 angle resolution for 20 cm gap and 0.5^0 for 50 cm gap (assuming one has a 0.3 cm vertical resolution).
Then, it is important to study the muon range in steel. It will provide information on the energy loss and the momentum of the incoming muon. Furthermore, it will help defining the thickness of the magnetic modules. For now, the muon range gives the momentum with a resolution of 50 MeV. This uncertainty can modify the shape of the angle distribution, but it has been studied and it has no relevant effect on the result of charge identification.
The main problem is the area where the angle distribution of μ^- and μ^+ overlap. The Lever-arm algorithm uses the distribution of deflection angle as a probability function of measured values of the angle with a fixed momentum. The Lever-arm uses these probability and compare them as follows :

$$\frac{\prod_{i=1}^{n} f_{\mu^-}(\Delta_i)}{\prod_{i=1}^{n} f_{\mu^+}(\Delta_i)} \tag{9}$$

With $f_{\mu^-}(\Delta_i), f_{\mu^+}(\Delta_i)$ the probabily function for a μ^-,μ^+ to reach the final angle Δ with the track i. If the ratio is bigger than 1, it is identified as a μ^- and as μ^+ if it is smaller than 1.
The simulations show that the Lever-arm algoritm has higher charge identification for low momentum than SaRoMan. However, a gain of charge identification efficiency is possible by increasing the thickness of the magnetic modules which signify a loss in reconstruction efficiency. This work will be continued in order to finalize the configuration of modules in the detector and wil finally implement the algorithms of SaRoMan.

6 Conclusion

The Baby MIND project completes the T2K experiment as the WAGASCI downstream MRD. However, the modularity of its design allows it to take place in a lot of different experiment. The TASD modules have proven their efficiency in the beam test and could be re-used as a full detector.
The BabyMIND is still in development but its design is fixed now. Huge progress in the electronics have been made in the last months. The new FEB allows to take a lot more data in a shorter time lapse. The software of the FEB have still some bugs but the beam test allowed us to see those bugs and try to correct it. The data taken during the beam test are still in analysis, they should give a better understanding of the studies we have done with the evaluation board.
The Baby MIND have to be in J-PARC for the next year, which means that the detector must be finished before this time. There is still some unknow behaviour of the electronics mostly concerning the pedestal, but the project is in a good way.

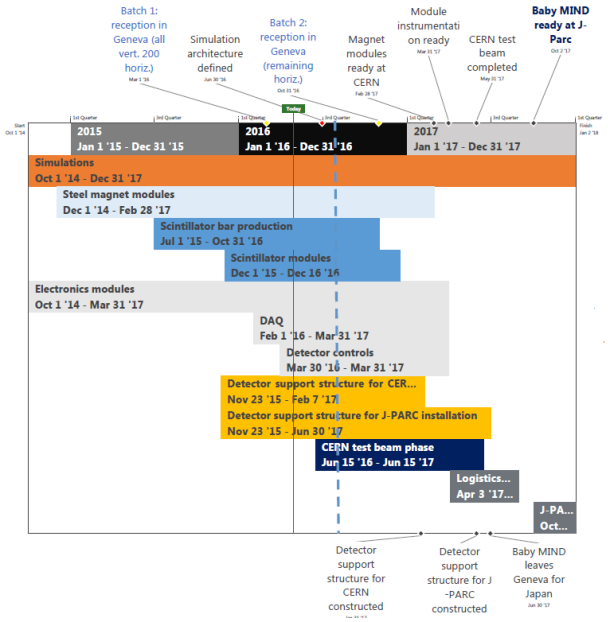

Figure 54: Baby MIND Schedule

7 Acknowledgements

This document was presented for the obtention of a master thesis at the University of Geneva. It was realised inside the neutrino group of the University under the supervision of the Professeur Alain Blondel and Etam Noah Messomo.
I would like to thank the Professeur Alain Blondel to have allowed me to take part in the Baby MIND project and discover the world[32] of the physics research.
I would like to especially thank the MA Etam Noah Messomo who was daily with me on this project and that, I hoped, I have helped a little. It was nice to learn and work beside him.
I would like to thank the all the BabyMIND collaboration without which there would have been no project. I would like to thank particularly the Japanese collaboration and the University of Glasgow for their reception. A special thank to Patrik with who we spent some night in the beam zone, trying to get the Baby MIND on the leaderboard.
Eventually, I am thankful to my friends, my family and my girlfriend who supported me all this time.

[32] literally in fact by the two trip I had to do for the project

List of Figures

List of Tables

References

[1] P. Lipari, INTRODUCTION TO NEUTRINO PHYSICS, Universita di Roma "la Sapienza", and I.N.F.N., Sezione di Roma, P.A. Moro 2, I-00185 Roma, Italy

[2] The T2K experiment, *t2k-experiment.org*

[3] Warwick University, The T2K experiment *www2.warwick.ac.uk*

[4] K. Abe et al. Nuclear Instruments and Methods in Physics Research, Section A: Accelerators, Spectrometers, Detectors and Associated Equipment volume 659, Issue 1, 2011

[5] Yasuyuki Yamazaki. The jaeri-kek joint project for the high-intensity proton accelerator, j-parc. In *Particle Accelerator Conference, 2003. PAC 2003. Proceedings of the*, volume 1, pages 576-580. IEEE, 2003.

[6] K. Abe et al. The T2K Neutrino Flux Prediction. *arXiv:1211.0469v3 hep-ex*, 22 Jan 2013

[7] Y. Fukuda, T. Hayakawa, E. Ichihara, M. Ishitsuka, Y. Itow, et al., Nuclear Instruments and Methods in Physics Research A 501 (2003) 418

[8] A. Pla-Dalmau, A. Bross, K.Mellott, Low-cost extruded plastic scintillator in *Nuclear Instruments and Methods in Physics Research A 466 (2001) 482–491*

[9] M. Yokoyama, et al., Nuclear Instruments and Methods in Physics Research A 622 (2010) 567.

[10] F. Moreau, et al., Nuclear Instruments and Methods in Physics Research A 613 (2010) 46.

[11] K. Abe et al. Measurements of the T2K neutrino beam properties using the INGRID on-axis near detector. *arXiv:1111.3119v1 physics.ins-det*, 14 Nov 2011

[12] T. Ovsiannikova, M. Antonova, C. Bronner, A. Blondel et al. The new experiment WAGASCI for water to hydrocarbon neutrino cross section measurement using the J-PARC beam in *Journal of Physics : Conference Series* volume 675, number 1, 2016.

[13] T. Koga et al. Water/CH Neutrino Cross Section Measurement at J-PARC (WAGASCI Experiment) in *JPS Conf. Proc.*, 023003 (2015)

[14] A. Minamino, New experimental proposal for neutrino cross sections with J-PARC neutrino beam WAGASCI, Conference at *NuInt14*, 22 May 2014, Surrey UK

[15] E. Noah, The WAGASCI experiment at J-PARC, *EPS-HEP2015* July 2015, Vienna Autria

[16] T. Hayashino, The WAGASCI experiment at J-PARC to measure the neutrino cross-section ratio between water and plastic, Conference at *TAUP2015*, 9 September 2015, Trino Italy

[17] M. Antonova, R. Asfandiyrov et al. Proposal for characterization of muon spectrometers for neutrino beam lines with the Baby MIND, CERN-SPSC-2015-031 / SPSC-P-353 2015

[18] Hamamatsu *http://www.hamamatsu.com/*

[19] Kuraray Specification *http://kuraraypsf.jp/psf/index.html*

[20] Y. Favre, Baby MIND Front End Electronics Specification v. 1.1, 24 June 2016

[21] CITIROC datasheet from Omega

[22] D. Impiombato et al. Characterization and performance of the ASIC (CITIROC) front-end of the ASTRI camera, *arXiv:1506.00264v1 physics.incs-det* 31 May 2015

[23] L. Durieu, M. Martini and A.-S. Müller, OPTICS STUDIES FOR THE T9 BEAM LINE IN THE CERN PS EAST AREA SECONDARY BEAM FACILITY in *Particle Accelerator Conference* at Chicago (2001)

[24] Saroman release URL : https://github.com/rbayes/SaRoMaN/tree/Release

[25] A. Cervera-Villanueva, J. J. Gomez-Cadenas, and J. A. Hernando, RecPack, a general reconstruction toolkit in *Astroparticle, Particle, Space Physics and Detectors For Physics Applications - Proceedings of the 13th ICATPP Conference. Edited by Giani Simone et al. Published by World Scientific Publishing Co. Pte. Ltd., 2012. ISBN 9789814405072, pp. 954-960.* Ed. by S. Giani et al. Aug. 2012, pp. 954-960.